Available online at www.sciencedirect.com
ScienceDirect
Chemical Geology 248 (2008) 40–61
CHEMICAL GEOLOGY INCLUDING ISOTOPE GEOSCIENCE
www.elsevier.com/locate/chemgeo

Mantle dynamics beneath East Asia constrained by Sr, Nd, Pb and Hf isotopic systematics of ultramafic xenoliths and their host basalts from Hannuoba, North China

Sung Hi Choi [a,b], Samuel B. Mukasa [a,*], Xin-Hua Zhou [c], Xiangyang Helena Xian [a], Alexandre V. Andronikov [a]

[a] *Department of Geological Sciences, The University of Michigan, 2534 C.C. Little Building, 1100 N. University, Ann Arbor, MI 48109-1005, USA*
[b] *Korea Polar Research Institute, Songdo Techno Park 7-50, Songdo-dong, Yeonsu-gu, Incheon 406-840, South Korea*
[c] *Laboratory of Lithosphere Tectonic Evolution, Institute of Geology and Geophysics, Chinese Academy of Science, Beijing 100029, China*

Received 7 May 2007; received in revised form 7 October 2007; accepted 16 October 2007

Editor: B. Bourdon

Abstract

We have determined the Sr, Nd, Pb and Hf isotopic compositions of clinopyroxene separated from mantle-derived ultramafic xenoliths (six spinel peridotites, two composite Cr-diopside pyroxenites, and one discrete Al-augite pyroxenite) hosted by Cenozoic alkali basalts at Hannuoba, North China, in order to understand the nature of the mantle source for this intraplate volcanism, and the petrologic history of the mantle lithosphere beneath North China Block, a crustal segment of the Sino-Korean Craton.

Measured Sr, Nd, Pb and Hf isotopic compositions in the clinopyroxene grains separated from spinel peridotite and Cr-diopside pyroxenite ($^{87}Sr/^{86}Sr$=0.70265 to 0.70485; $^{206}Pb/^{204}Pb$=17.75 to 19.15; ε_{Nd}=0 to +11; ε_{Hf}=+10 to +38) display mixing hyperbolas between mantle compositional end members DMM and EMII on the Sr–Pb and Nd–Pb isotope correlation diagrams. This is distinctly different from the host basalt data which show a mixture of DMM and EMI components on the diagrams. We interpret this to reflect infiltration by metasomatic agents, possibly silicate melts, having an EMII-like isotopic signature, which enriched a precursor time-integrated depleted mantle.

An Al-augite pyroxenite, also hosted by these basalts, is characterized by highly enriched Sr, Nd, and Hf isotopic compositions ($^{87}Sr/^{86}Sr$=0.70733; ε_{Nd}=−16; ε_{Hf}=−18) with only moderately radiogenic Pb that has a $^{206}Pb/^{204}Pb$ value of 18.23. All of these data plot outside (1) the fields for oceanic basalts, and (2) the mixing arrays defined on the isotopic correlation diagrams by peridotites/Cr-diopside pyroxenite with their metasomatic agents, and by the host basalt. These observations suggest that (1) Al-augite pyroxenite is not cogenetic with the Cr-diopside pyroxenite, (2) parental melts of the pyroxenites are not likely to be the source for the metasomatism, and (3) the thermo/mechanically reactivated pyroxenite and/or spinel peridotite, is not likely to be the source for host basalt magmatism. The Cenozoic intraplate volcanism, therefore, must have originated in the asthenosphere.

We observe that the relatively little-metasomatized Hannuoba peridotites define a Lu–Hf isochron of 2587±86 Ma (2σ). This value is, within error, indistinguishable from the Sm–Nd isochron age of the overlying granulite terrain. We suggest, therefore, that the Lu–Hf system can be used to constrain the timing of lithospheric mantle differentiation. Preservation of the Neoarchean mantle

* Corresponding author. Tel.: +1 734 936 3227; fax: +1 734 763 4690.
E-mail address: mukasa@umich.edu (S.B. Mukasa).

0009-2541/$ - see front matter
doi:10.1016/j.chemgeo.2007.10.008

lithosphere beneath Hannuoba, despite the protracted tectono-magmatic reactivation during the Mesozoic and Cenozoic in this area, suggests that complete removal of the lithospheric mantle beneath East Asia by wholesale delamination is unlikely.

Keywords: Sr, Nd, Pb and Hf isotope; Ultramafic xenoliths; Neoarchean; Hannuoba; China

1. Introduction

The mantle source for the Late Cenozoic intraplate volcanism in East Asia has been characterized by two large-scale isotopic domains: DMM (depleted mantle)–EMI (enriched mantle type 1) for northeast China and western Korea, and DMM–EMII (enriched mantle type 2) for Southeast Asia (e.g., Zou et al., 2000; Choi et al., 2006a). Previous studies in eastern China, based on comparison of the Paleozoic kimberlite-borne and Cenozoic basalt-borne mantle xenoliths, have suggested that thick, cold, and refractory Archean lithospheric keel that existed beneath the eastern block of the North China Craton has been removed and replaced by thin, hot and relatively less refractory post-Archean lithospheric mantle (e.g., Menzies et al., 1993; Griffin et al., 1998; Fan et al., 2000; Gao et al., 2002; Zhang, 2005). Although the timing, extent and mechanisms (delamination, thermal/chemical erosion or simple rifting) of thinning the lithospheric mantle beneath the North China Craton are yet to be fully understood (e.g., Zheng et al., 1998; O'Reilly et al., 2001; Gao et al., 2002; Wilde et al., 2003), it has been generally invoked that the thermo/mechanically reactivated endogenous subcontinental lithospheric mantle (SCLM) is likely to be the source for the enriched end member components of EMI and EMII for the intraplate volcanism in East Asia (e.g., Tatsumoto et al., 1992; Hoang et al., 1996; Zhang et al., 1998; Chung 1999; Zou et al., 2000). Therefore, defining the isotopic characteristics and constraining the age of differentiation events in the SCLM beneath East Asia is important to clear the issue.

Hannuoba basalts in Hebei Province, North China Craton (Fig. 1) carry a remarkable variety of deep-seated xenoliths from the lower crust and upper mantle, including mafic to felsic granulites, spinel-and garnet-bearing pyroxenites, abundant spinel peridotites, and some rare garnet–spinel peridotites, which have been the subject of a number of petrological and geochemical studies (e.g., Song and Frey, 1989; Tatsumoto et al., 1992; Fan et al., 2000; Chen et al., 2001; Liu et al., 2001; Gao et al., 2002; Xu, 2002; Zhou et al., 2002; Wilde et al., 2003; Rudnick et al., 2004; Liu et al., 2004, 2005). A number of studies (e.g., Song and Frey, 1989; Tatsumoto et al., 1992; Fan et al., 2000; Rudnick et al., 2004) reported Sr and Nd isotopic compositions for the Hannuoba peridotite xenoliths, but these do not clearly distinguish between the EMI and EMII mantle end members. Tatsumoto et al. (1992) reported a few Pb isotopic ratios for them, but that work was too limited in scope to fully characterize the nature of the lithospheric mantle beneath Hannuoba. More recently, Gao et al. (2002) suggested that lithospheric delamination beneath Hannuoba might have occurred as long ago as the Paleoproterozoic, with the replacement mantle lithosphere remaining intact all the way through the time of Hannuoba basalt eruption, based on the ~1.9 Ga Re–Os errorchron for the spinel peridotite xenoliths.

It has been demonstrated in a number of studies that the Lu–Hf system is not as easily reset as the Sm–Nd system by some younger metamorphic and metasomatic events because (i) Hf has a considerably smaller diffusivity in silicate minerals than do Nd or Pb, and (ii) the relative difference in Hf concentration between melt and peridotite is lower than of the relative difference in Nd concentration for the same materials (e.g., Pearson and Nowell, 2003; Choi et al., 2006b; Bizimis et al., 2007). Our goal in this study, therefore, has been to constrain the petrologic history of the lithospheric mantle beneath Hannuoba using a variety of isotopic methods, in order to better understand the overall geodynamic development of the upper mantle beneath East Asia. Our approach has been to determine the Sr, Nd, Pb and Hf isotopic compositions for the Hannuoba mantle-derived xenoliths (spinel peridotites and pyroxenites) and the host alkali basalts, and then using the results in conjunction with elemental concentration data to decipher source characteristics and melting processes. The discussion that follows, therefore, will focus on the mantle source (lithospheric vs. asthenospheric) for the host basalts, the depletion age of the peridotite protoliths, the nature of secondary metasomatizing agents that the data seem to require, and the origin of the pyroxenites. We argue that the host basalt volcanism and the metasomatizing agents that overprinted the mantle-derived xenoliths were both

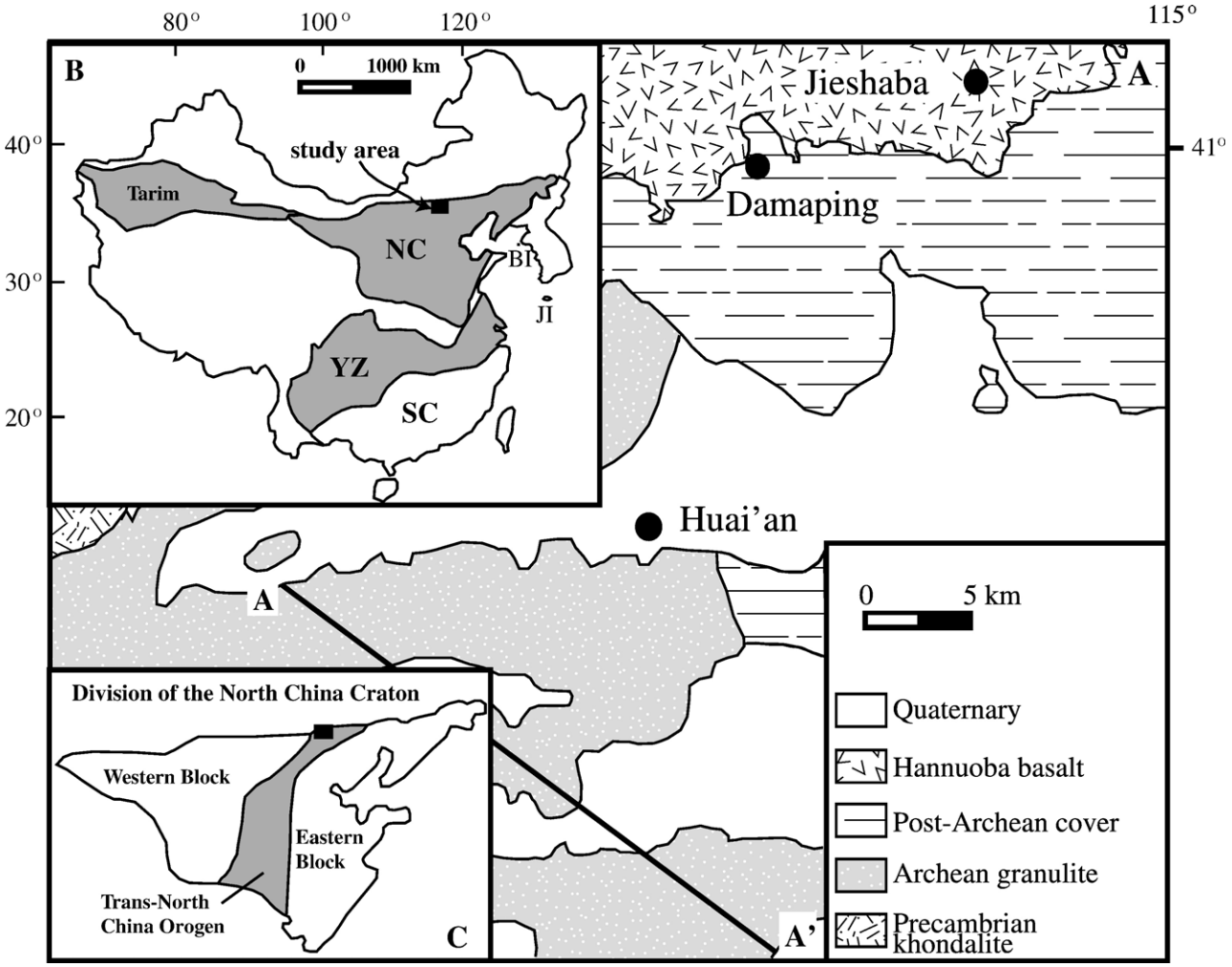

Fig. 1. (A) Simplified geological map of the Hannuoba area, after Liu et al. (2004). A–A′ is the sampling profile for the Archean terrain granulites from Liu et al. (2004). Inset (B) shows location of the study area and tectonic division of China, after Zhao et al. (2001), and (C) division of the North China Craton. NC: North China Craton, YZ: Yangtze Craton, SC: South China orogen, BI: Baengnyeong Island, and JI: Jeju Island.

sourced in the asthenosphere. We also show that the Lu–Hf method provides better age constraints than other methods, such as Sm–Nd, on the timing of lithospheric mantle differentiation.

2. Geological setting and petrography of the xenoliths studied

The North China Craton can be divided into three blocks: the Eastern Block, the Western Block and the intervening Trans-North China Orogen (Central Orogenic Belt), based on geochronological data, lithological assemblages, tectonic evolution, and *P–T–t* paths (Fig. 1C) (Zhao et al., 2000, 2001). Late Archean basement rocks which consist dominantly of 2.6–2.5 Ga TTG gneisses, ultramafic to mafic igneous rocks, ~2.5 Ga syntectonic granites and a variety of supracrustal rocks are widespread in the North China Craton, and make up 85% of the total exposure of Archean basement (Zhao et al., 2001). Early to Middle Archean (3.85–3.2 Ga) basement rocks are only present in the Eastern Block. The Trans-North China Orogen is in fault contact with both the Eastern and Western blocks, and is composed of reworked Archean materials derived from the two blocks, as well as Late Archean to Paleoproterozoic juvenile igneous and sedimentary rocks, including a series of 2.5–2.7 Ga amphibolite to granulite facies terrains (e.g., Huai'an; Fig. 1A) (Kröner et al., 1988; Kern et al., 1996; Zhao et al., 2000, 2001).

Zhao et al. (2001) and Wilde et al. (2002) suggested, on the basis of geochronology in conjunction with the clockwise *P–T–t* paths computed for metamorphic

rocks, that final amalgamation of the Western and Eastern blocks occurred at ~1.8 Ga during a continent–continent collisional episode along the Central Orogenic Belt, resulting in closure of an ancient ocean basin. The North China Craton experienced widespread tectonothermal reactivation during the Late Mesozoic and Cenozoic as indicated by the emplacement of voluminous Late Mesozoic silicic intrusions and volcanic rocks (Shao et al., 2001; Meng, 2003; Yang et al., 2003; Zhang, 2005), as well as extensive Tertiary alkali basaltic volcanism (Zhou and Armstrong, 1982; Zou et al., 2000).

The Hannuoba volcanic field is located near the northern margin of the Trans-North China Orogen (Fig. 1C) and covers up to 1700 km^2. It consists of interlayered alkali basalt and tholeiite, with the former carrying a variety of mantle and crustal xenoliths. Dated at 14–27 Ma by the K–Ar method (Zhu, 1998), this basaltic volcanism is thought to be related to widespread Cenozoic rifting in the North China Craton (Basu et al., 1991). The xenoliths studied were collected from lava flows at the Damaping and Jieshaba localities (Fig. 1A). The Damaping lavas were erupted through the Archean Huai'an granulite terrain (Gao et al., 2002) which is thought to represent an exposed lower crustal section (Zhai, 1996).

We selected five spinel lherzolite, one spinel harzburgite, and three pyroxenite xenoliths to represent as wide a range of rock types as possible for this isotopic study. The spinel peridotite xenoliths we have investigated belong to Group I of Frey and Prinz (1978), essentially anhydrous peridotite consisting of

Table 1
Whole-rock major and trace element concentrations for ultramafic xenoliths from Hannuoba, North China

Sample No.	DM-1-Hz	DM-1-Px	95DA58-Lz	95DA58-Px	95DA101	95DA105	95DA118	95JSB2
Rock type	Sp. Harzburgite	Websterite	Sp. Lherzolite	Websterite	Sp. Lherzolite	Sp. Lherzolite	Sp. Lherzolite	Websterite
SiO_2 (wt.%)	43.94	51.81	44.77	52.45	45.18	43.72	44.12	50.55
TiO_2	0.03	0.17	0.09	0.16	0.32	0.16	0.18	0.57
Al_2O_3	1.41	4.96	2.61	4.53	4.12	3.08	2.15	4.54
Fe_2O_3[a]	8.97	4.38	8.09	3.47	8.48	8.90	8.46	9.69
MnO	0.14	0.10	0.12	0.09	0.13	0.13	0.12	0.14
MgO	43.60	22.04	40.84	19.92	37.40	40.31	42.48	20.49
CaO	1.06	14.16	2.12	16.53	3.26	2.22	1.41	12.72
Na_2O	0.14	0.74	0.05	1.07	0.24	0.10	0.04	0.62
K_2O	0.00	0.01	0.00	0.00	0.01	0.01	0.06	0.11
P_2O_5	0.00	0.00	0.03	0.03	0.01	0.05	0.04	0.05
Total	99.3	98.4	98.7	98.3	99.2	98.7	99.1	99.5
Mg#[b]	90.6	90.9	90.9	91.9	89.7	90.0	90.9	80.7
Cr (ppm)	3165	9394	3142	6823	2579	2816	2665	1856
Ni	2284	1105	2442	617	2372	2472	2536	789
Cu	21.0	128.0	16.2	37.1	62.5	50.0	36.0	154.5
Zn	50.0	26.0	44.2	19.9	49.1	50.4	45.8	56.9
V	41.0	184.0	n.d.	n.d.	n.d.	n.d.	n.d.	n.d.
Rb	n.d.	n.d.	n.d.	3.2	n.d.	n.d.	n.d.	5.3
Sr	6.0	34.0	26.7	103.1	22.0	23.8	28.2	82.7
Zr	1.0	5.0	12.7	18.9	17.4	14.2	16.1	29.2
Nb	n.d.	n.d.	6.5	8.3	6.8	8.0	6.4	5.0
La	n.d.	n.d.	8.5	16.7	n.d.	n.d.	11.8	9.5
Modal mineralogy (vol%)								
Olivine	70.6	1.0	60.4	1.5	49.7	63.2	65.1	2.0
Orthopyroxene	24.6	31.3	28.8	22.2	32.8	25.1	28.2	41.4
Clinopyroxene	4.0	66.3	8.8	75.9	15.5	10.0	5.5	56.6
Spinel	0.8	1.4	2.0	0.5	2.0	1.8	1.2	–

Modes were calculated by least-squares fit of the whole-rock major element compositions to the mean core compositions of olivine, orthopyroxene, clinopyroxene, and spinel (Tables 5–8; Chen et al., 2001, and Mukasa, unpublished data). The compositions of SiO_2, TiO_2, Al_2O_3, Cr_2O_3, ∑FeO, MnO, MgO, NiO, CaO and Na_2O were considered. For classification, the least-squares-derived mineral proportions (wt.%) were converted to vol%, on the assumption of the following specific gravities: olivine, 3.3; pyroxenes, 3.2; spinel, 4.5.

n.d. = not determined.

Sp. = spinel.

[a]All Fe reported as Fe_2O_3.

[b]100 Mg/(Mg+∑Fe).

olivine, orthopyroxene, clinopyroxene and spinel as the principal phases. The pyroxenites (websterites) studied are divided into Al-augite and Cr-diopside series after Wilshire and Shervais (1975). The Cr-diopside websterite veins (DM-1-Px and 95DA58-Px) occur as composite xenoliths with spinel peridotite (DM-1-Hz and 95DA58-Lz, respectively), having sharp contacts between the two lithologies. The Al-augite websterite (95JSB2) occurs as a discrete nodule, but Xu (2002) reported samples of this series to also occur as composite xenoliths with peridotite.

The modal mineralogy of the xenoliths, determined from calculations using bulk rock chemistry (Table 1) and mineral compositions (Tables 5–8; Chen et al., 2001) is listed in Table 1. The lherzolites contain 50–65% olivine, 25–33% orthopyroxene, 6–16% clinopyroxene, and 1–2% spinel, and the harzburgite 71% olivine, 25% orthopyroxene, 4% clinopyroxene and 1% spinel. The Cr-diopside websterites consist of clinopyroxene (66–76%) and orthopyroxene (22–31%) with minor olivine (1–2%) and spinel (1–2%). Al-augite websterite (95JSB2) is composed of clinopyroxene (57%) and orthopyroxene (41%) with minor olivine (2%). Spinel peridotites have typical grain sizes in the range of 2–4 mm, and overall exhibit a protogranular texture. Olivine in sample DM-2 has been partly serpentinized. The websterites have a typical grain size of 2–3 mm, and exhibit a granular texture with no grain deformation. Clinopyroxene in the websterites has exsolved orthopyroxene lamellae, implying sub-solidus re-equilibration. Petrography and mineral chemistry for the samples studied were reported in Chen et al. (2001). Application of the two-pyroxene thermometer of Wells (1977) yields an equilibrium temperature range of 820–960 °C (Table 2), and there are no discernable differences in temperature between peridotites and Cr-diopside/Al-augite websterites, further indicating a mantle origin for the pyroxenite xenoliths along with their being attached to peridotite to form a composite xenolith. Petrography and geochemistry for the host alkali basalts appeared in Song et al. (1990), Zhi et al. (1990), and Basu et al. (1991). The basalts display an oceanic island basalt-like geochemical signature, ruling out the possibility of significant crustal contamination. Furthermore, the high abundance of ultramafic xenoliths in the basalts supports the notion that ascent speeds were rapid, living little chance for crustal contamination to occur.

3. Analytical methods

Samples for whole-rock analysis were prepared from the core of each xenolith, free of any visible surface

Table 2
Trace element concentrations (ppm) for ultramafic xenoliths from Hannuoba, North China

Sample no.	DM-1-Hz	DM-1-Px	DM-32	95DA58-Lz	95DA58-Px	95DA101	95DA105	95DA118	95JSB2
Rock type	Sp.Hz.	Websterite	Sp.Lz.	Sp.Lz.	Websterite	Sp.Lz.	Sp.Lz.	Sp.Lz.	Websterite
Analysis	cpx	cpx	cpx	cpx	cpx	cpx	cpx	cpx	cpx
Ti	1241	1204	4901	1396	1107	3244	2116	1434	4352
V	224	231	314	229	194	255	230	211	232
Cr	8142	8377	5477	8555	10654	4534	5912	7480	2759
Sr	54.2	57.5	24.5	114.3	113.0	73.1	98.6	91.6	130.3
Y	7.0	7.1	27.6	7.5	6.7	17.4	13.7	7.0	9.6
Zr	8.1	7.6	65.9	12.4	9.6	35.1	21.3	11.3	20.8
La	0.97	0.95	2.08	7.21	5.81	1.02	3.36	4.03	1.30
Ce	2.85	3.05	7.19	12.89	10.39	4.15	5.63	6.86	7.30
Nd	3.05	2.85	6.58	6.75	4.07	3.89	3.54	2.58	8.71
Sm	1.69	1.36	3.01	1.64	1.26	1.70	1.55	0.93	3.09
Eu	0.46	0.46	0.95	0.48	0.33	0.55	0.65	0.34	1.12
Dy	1.34	1.44	4.13	1.38	0.95	2.68	2.54	1.15	1.97
Er	0.96	0.92	2.48	0.85	0.72	1.83	1.72	0.73	1.02
Yb	0.89	0.93	2.40	0.90	0.73	1.71	1.65	0.75	1.03
$(La/Yb)_N$	0.78	0.73	0.62	5.73	5.72	0.43	1.46	3.87	0.91
Fo_olivine	90.5 (90.6[b])	90.5[b]	88.7 (89.0[b])	90.5 (90.8[b])	90.7[b]	89.8 (89.7[b])	89.8 (90.2[b])	90.7 (90.9[b])	78.8
Cr#_spinel	25.6 (25.7[b])	24.5[b]	7.7 (8.2[b])	21.4 (21.0[b])	32.3[b]	9.2 (9.6[b])	13.9 (13.6[b])	27.5 (26.4[b])	–
T (°C)[a]	867[b]	886[b]	961[b]	820[b]	826[b]	960[b]	945[b]	953[b]	852[b]

Cr# = 100Cr/(Cr+Al).
Abbreviations: Sp.Lz. = spinel lherzolite, Sp.Hz. = spinel harzburgite, cpx = clinopyroxene.
[a]Determined by two-pyroxene thermometer of Wells (1977).
[b]Data from Chen et al. (2001).

weathering, using standard procedures of jaw-crushing pre-cleaned rock chips. To avoid the effects of infiltration by the magmas that carried the xenoliths to the surface or alteration by near-surface fluid, we limited our isotopic analyses to ultra-pure clinopyroxene separates. Clinopyroxene is the major carrier of REE, Sr, Pb and possibly Hf in the anhydrous spinel peridotite and spinel websterite mineral assemblages (e.g., Zindler and Jagoutz, 1988; Reisberg et al., 1989; Mukasa and Wilshire, 1997; Bizimis et al., 2003a), and therefore, we treat the data for this mineral as representative of each xenolith. Clinopyroxene grains were prepared from unweathered samples using nylon sieves for sizing, a magnetic separator to eliminate grains with dark inclusions, and hand picking under a binocular microscope to select only the optically clear grains for analysis. Prior to dissolution for the isotopic analyses, the minerals were washed in warm, distilled 2.5 N HCl for 15 min., and in warm distilled 5% HF for 15 min., with an H_2O rinse after each of these steps.

Major element and selected trace element concentrations were determined by X-ray fluorescence (XRF) spectrometry on fused disks at Michigan State University, following procedures described in Hannah et al. (2002). Standards (JB-1a-1, JB-1a-5 and W-2) were analyzed with the unknown samples, as reported in Choi et al. (2006a). The data were reduced by weighted regression using compiled analyses on the standard materials. Precision was estimated to be within 5%. The results are presented in Table 1.

Trace element concentrations in clinopyroxene have been measured in thin sections with a CAMECA IMS-3f ion microprobe at the Woods Hole Oceanographic Institution. Details about the operating conditions, analytical errors, and standardization scheme for this instrument are described by Shearer et al. (1990). Well-documented standard KH-1 CPX (Irving and Frey, 1978) has been used to correct for matrix effects on ion yield in calculating the working curves. Secondary intensities (I) of REEs were normalized to ^{30}Si to produce I(REE)/I(^{30}Si) vs. REE (concentration) working curves. The results are given in Table 2.

Sr, Nd and Pb isotope analyses, including chemical separation and measurements on VG Sector thermal ionization mass spectrometers, were performed at the University of Michigan. Details of the analytical procedures appear in Mukasa et al. (1987, 1991). ^{87}Sr/^{86}Sr and ^{143}Nd/^{144}Nd ratios were corrected for instrumental mass fractionation by normalizing to ^{86}Sr/^{88}Sr=0.1194 and ^{146}Nd/^{144}Nd=0.7219, respectively. Replicate analyses of NBS-987 and La Jolla standards gave ^{87}Sr/^{86}Sr=0.710255±11 (N=30, 2σ) and ^{143}Nd/^{144}Nd=0.511848±19 (N=30, 2σ). Measured Pb isotopic ratios were corrected for instrumental mass fractionation of 0.1% per atomic mass unit by reference to replicate analyses of the standard NBS-981. Total blanks averaged 0.2 ng for Sr, 0.04 ng for Nd, and 0.02 ng for Pb. The results are given in Table 3.

The Hf isotope analyses were determined with the multiple-collector ICP-MS (Nu-Plasma HR) at the University of Michigan, after column separation procedures summarized by Münker et al. (2001). Lu and Hf concentrations were measured by isotope dilution with enriched ^{176}Lu and ^{178}Hf spikes. In order to monitor machine performance, the JMC-475 standard was run after every three samples obtaining a mean ^{176}Hf/^{177}Hf ratio of 0.282146±8 (N=9, 2σ), and the values reported were normalized to the accepted value of 0.282160. The total procedural blank level was about 20 pg for Hf. The results are given in Table 3.

4. Results and interpretations

4.1. Whole-rock chemistry

The whole-rock *mg-numbers* (=100 Mg/(Mg+∑Fe)) of the Hannuoba peridotites studied have a range of 89.7–90.9 (Table 1). Variations in representative major oxide (Al_2O_3, CaO and SiO_2) as a function of MgO, good indicators of the degree of depletion of the peridotites, are shown in Fig. 2A–C. Available data from previous studies (Song and Frey, 1989; Chen et al., 2001; Rudnick et al., 2004) are also shown for comparison. The Hannuoba peridotites are characterized by a wide range of compositional variation, extending from primitive mantle-like to average abyssal peridotite values (Fig. 2A–C). Our samples cover this entire Hannuoba peridotite compositional range, which is why we selected them for isotopic study. The abundance and trends illustrated in Fig. 2A–C are compatible with the best-fit lines for world-wide spinel peridotite xenolith compositions, suggesting that the rocks are residues following variable basaltic melt extraction.

The whole-rock *mg-numbers* for Cr-diopside websterite range from 90.9 to 91.9, while the Al-augite websterite has a significantly lower value of 80.7. The websterites have higher Al_2O_3, Na_2O, CaO and SiO_2 contents compared to the peridotites, and this relationship holds true for the Cr and Sr concentrations as well (Table 1). However, Cr-diopside websterite has lower Ni concentrations compared to the host lherzolite. The compositional ranges of the two websterite series studied fall within the range reported by Xu (2002) for the Hannuoba Cr-diopside and Al-augite series

Table 3
Sr–Nd–Pb–Hf isotopic compositions for ultramafic xenoliths from Hannuoba, North China

Sample no.	DM-1	DM-32	95DA58-Lz	95DA58-Px	95DA101	95DA105	95DA118	95JSB2	95JSB2	95DA41	DA20-43	DA20-57
Rock type	Sp. Hz.	Sp. Lz.	Sp. Lz.	Websterite	Sp. Lz.	Sp. Lz.	Sp. Lz.	Websterite	Websterite	Alkali basalt	Alkali basalt	Alkali basalt
Analysis	cpx	cpx	cpx	cpx	cpx	cpx	cpx	cpx	wr	wr	wr	wr
[Rb] ppm	0.003	0.009	0.025	0.068	0.004	0.002	0.002	0.008	1.137	n.d.	n.d.	n.d.
[Sr] ppm	45.9	74.5	65.3	119.5	65.4	101.2	83.6	111.7	75.8	n.d.	n.d.	n.d.
$^{87}Rb/^{86}Sr$	0.0002	0.0004	0.0011	0.0016	0.0002	0.0001	0.0009	0.0002	0.0434	n.d.	n.d.	n.d.
$^{87}Sr/^{86}Sr \pm 2\sigma$	0.703129±14	0.703048±23	0.704074±17	0.704001±18	0.702652±21	0.702901±20	0.704845±21	0.707327±20	0.707086±20	0.703954±14	0.704758±15	0.704201±17
$(^{87}Sr/^{86}Sr)_{t=150\ Ma}$	0.703129	0.703047	0.704072	0.703998	0.702652	0.702901	0.704843	0.707327	0.706993	–	–	–
[Sm] ppm	0.79	2.20	1.09	1.22	1.69	1.33	0.88	2.65	1.75	n.d.	n.d.	n.d.
[Nd] ppm	2.37	6.03	4.70	5.87	4.16	3.87	2.85	8.53	5.37	n.d.	n.d.	n.d.
$^{147}Sm/^{144}Nd$	0.2013	0.2205	0.1237	0.1258	0.2451	0.2075	0.1873	0.1878	0.1734	n.d.	n.d.	n.d.
$^{143}Nd/^{144}Nd \pm 2\sigma$	0.513044±18	0.513022±19	0.512806±19	0.512774±21	0.513143±18	0.513216±17	0.512653±18	0.511836±20	0.511980±19	0.512890±18	0.512907±18	0.512894±20
$(^{143}Nd/^{144}Nd)_{t=150\ Ma}$	0.512846	0.512806	0.512685	0.512651	0.512902	0.513012	0.512469	0.511652	0.511810	–	–	–
$(\varepsilon_{Nd})_{t=0}$	7.9	7.5	3.3	2.7	9.9	11.3	0.3	−15.6	−12.8	4.9	5.2	5.0
$(\varepsilon_{Nd})_{t=150\ Ma}$	7.8	7.0	2.3	4.0	8.9	11.1	0.5	−15.5	−12.4	–	–	–
T_{DM} (Ma)[a]	965	−1747	530	600	136	−3209	2803	7935	4383	–	–	–
[U] ppm	n.d.	n.d.	n.d.	n.d.	0.19	0.04	0.03	0.03	n.d.	n.d.	n.d.	n.d.
[Pb] ppm	0.12	0.05	0.13	0.35	0.35	0.12	0.28	0.70	n.d.	n.d.	n.d.	n.d.
$^{238}U/^{204}Pb$	n.d.	n.d.	n.d.	n.d.	34.53	18.29	7.66	2.33	n.d.	n.d.	n.d.	n.d.
$^{206}Pb/^{204}Pb$	18.26	18.19	18.80	19.13	17.75	17.99	19.15	18.23	18.27	17.94	17.89	17.95
$^{207}Pb/^{204}Pb$	15.50	15.51	15.56	15.63	15.53	15.52	15.71	15.51	15.49	n.d.	15.50	15.54
$^{208}Pb/^{204}Pb$	38.05	38.14	38.92	39.35	37.78	37.98	39.05	38.17	38.03	38.40	38.15	38.03
$(^{206}Pb/^{204}Pb)_{t=150\ Ma}$	–	–	–	–	16.94	17.56	18.97	18.18	–	–	–	–
[Lu] ppm	0.11	0.34	0.14	0.10	0.29	0.24	0.11	0.06	0.07	0.10	0.15	0.12
[Hf] ppm	0.35	1.60	0.43	0.26	1.21	0.74	0.48	0.47	0.68	7.05	5.73	5.74
$^{176}Lu/^{177}Hf$	0.0458	0.0301	0.0451	0.0512	0.0336	0.0462	0.0336	0.0176	0.0145	0.0020	0.0036	0.0029
$^{176}Hf/^{177}Hf \pm 2\sigma$	0.283461±27	0.283038±9	0.283729±20	0.283377±46	0.283231±9	0.283834±16	0.283061±34	0.282262±18	0.282418±18	0.283041±6	0.283035±6	0.282984±6
$(^{176}Hf/^{177}H)_{t=150\ Ma}$	0.283333	0.281954	0.283603	0.283233	0.283137	0.283705	0.282967	0.282213	0.282377	–	–	–
$(\varepsilon_{Hf})_{t=0}$	24.4	9.4	33.8	21.4	16.2	37.6	10.2	−18.0	−12.5	9.5	9.3	7.5
$(\varepsilon_{Hf})_{t=150\ Ma}$	23.1	9.7	32.7	19.6	16.2	36.3	10.2	−16.5	−10.7	–	–	–

The concentrations of Rb, Sr, Sm, Nd, U, Pb, Lu and Hf were determined by the isotope dilution technique.
Abbreviations: cpx = clinopyroxene, wr = whole-rock, Sp.Lz. = spinel lherzolite, Sp.Hz. = spinel harzburgite.
[a]Nd model ages calculated with assumed depleted mantle evolution parameters of $^{147}Sm/^{144}Nd = 0.2124$, $^{143}Nd/^{144}Nd = 0.513114$.

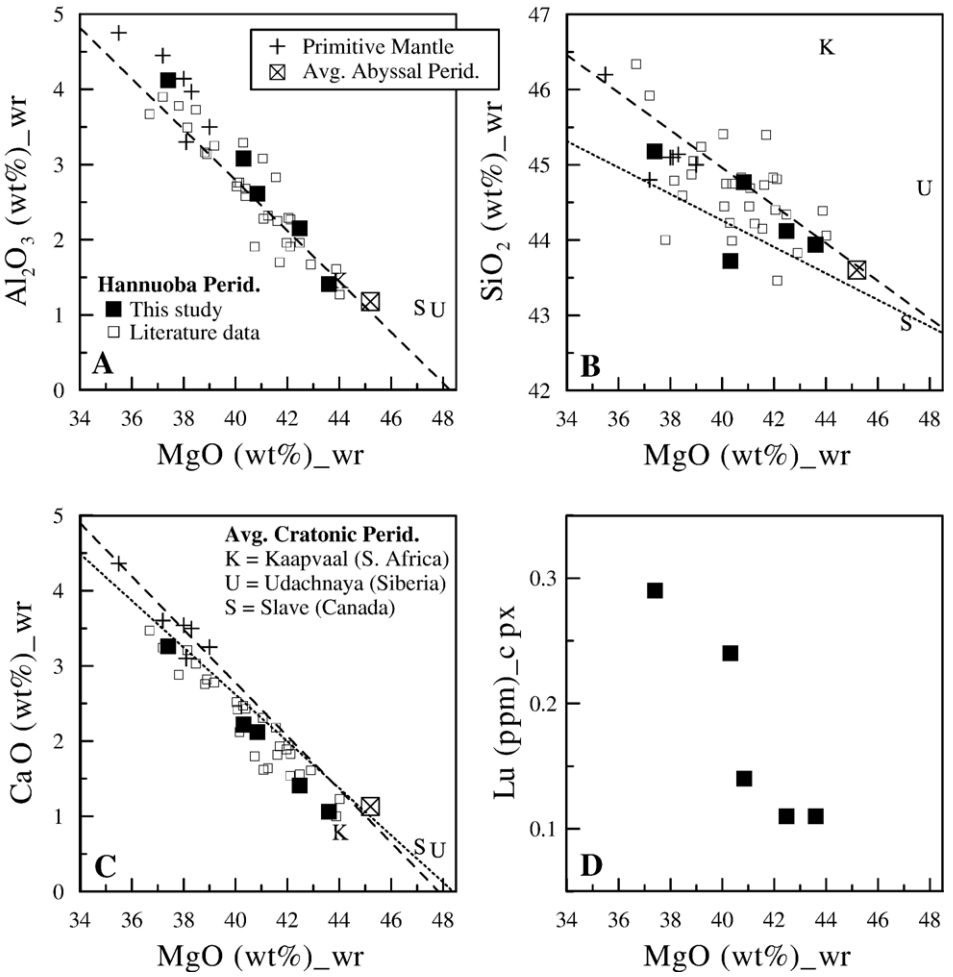

Fig. 2. Major element and Lu compositional variation diagrams for the Hannuoba peridotite xenoliths. The dashed lines are the best-fit lines for spinel lherzolite xenoliths elsewhere from Maalφe and Aoki (1977), and the dotted lines, from McDonough (1990). Literature data for the Hannuoba peridotites are from Song and Frey (1989), Chen et al. (2001), and Rudnick et al. (2004). Data sources: primitive mantle (Palme and Nickel, 1985; McDonough 1990 and references therein), average abyssal and Kaapvaal cratonic peridotites (Boyd, 1989), and average Udachnaya and Slave cratonic peridotites (Griffin et al., 1999). Abbreviations: cpx = clinopyroxene; wr = whole-rock.

pyroxenites, but are not on the same trend defined by the peridotites (not shown). Based on the geochemistry, Xu (2002) argued that the Hannuoba pyroxenites are not crystallized melts or representatives of a pyroxene-rich end-member of the residual peridotite suite, but rather that they are fractionally segregated products of melts at high pressure.

4.2. Rare earth element pattern of clinopyroxenes

Hannuoba peridotite clinopyroxene $(Yb)_N$ values, normalized to chondrite, are variable from 4.4 to 14.1 (Table 2). Heavy rare earth element (HREE) abundances (e.g., Yb and Lu) in the peridotites are negatively correlated with MgO concentrations (Tables 1–3; Fig. 2D), likely to represent variable degrees of partial melting during formation of the lithosphere. Chondrite-normalized REE patterns for the clinopyroxene grains from spinel peridotites are variable, from LREE-depleted (samples DM-32 and 95DA101) through spoon-shaped (sample 95DA105) to LREE-enriched (samples 95DA58 and 95DA118) (Fig. 3A–C). Sample DM-1 shows LREE-depleted but fractionated MREE with a negative slope and flat HREE pattern, with a maximum at Sm. All the Hannuoba peridotite clinopyroxene grains have flat HREE patterns, indicating that garnet was not involved in the source.

Clinopyroxene from Al-augite websterite shows a convex-upward REE pattern with an apex at Sm, which is typical of pyroxenite xenoliths in alkali basalts (e.g.,

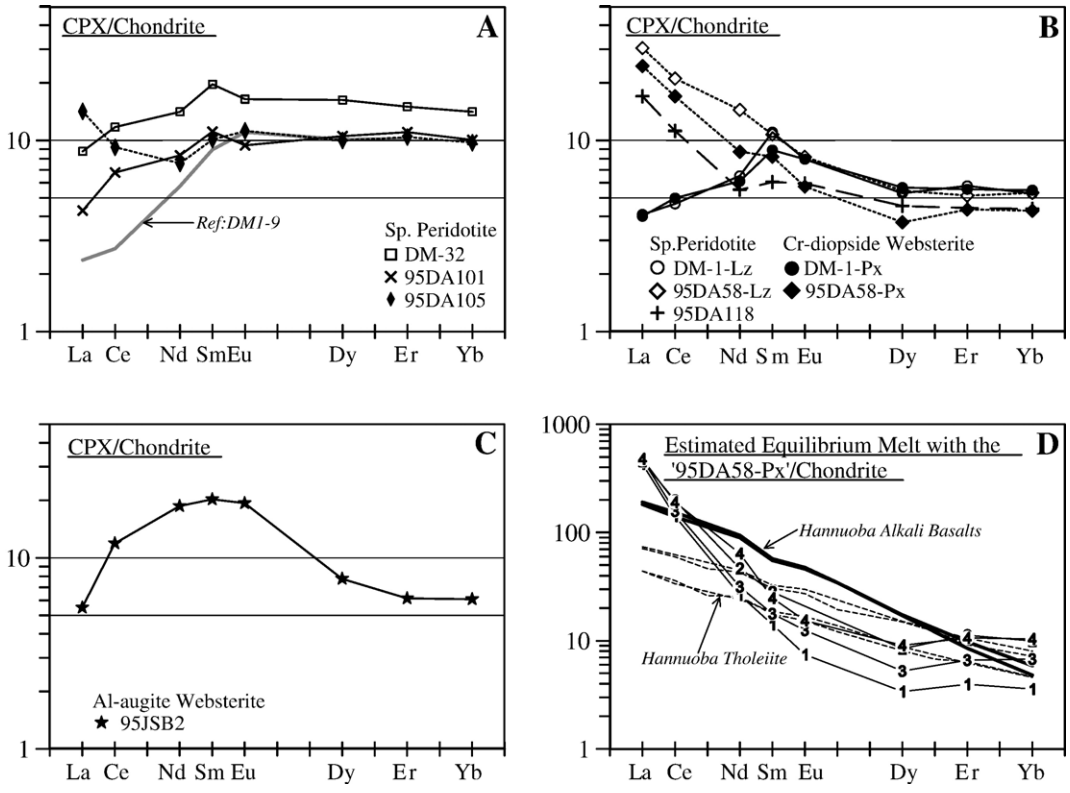

Fig. 3. (A–C) Rare earth element (REE) abundances of clinopyroxene from the Hannuoba ultramafic xenoliths, normalized to chondritic values (Sun and McDonough, 1989). Hannuoba reference sample DM1-9 in (A) is from Song and Frey (1989). (D) Calculated REE abundances of the hypothetical melts in equilibrium with clinopyroxene from sample 95DA58-Px. Partition coefficients for the clinopyroxene are from experimental runs at 1 = 1080°/2.0 GPa, clinopyroxene + orthopyroxene + melt as coexisting phases, Green et al. (2000); 2 = 1380°/3.0 GPa, clinopyroxene + melt, Hart and Dunn (1993); 3 = 1430°/2.5 GPa, clinopyroxene + garnet + melt, Hauri et al. (1994); and 4 = 1405°/1.7 GPa, clinopyroxene + melt, Hauri et al. (1994). The data for the Hannuoba tholeiite and alkali basalts (Liu et al., 1994) are also shown for comparison.

McDonough and Frey, 1989). This characteristic is attributed to equilibration with a basaltic melt, based on the clinopyroxene/liquid partition coefficients (Irving and Frey, 1984). Clinopyroxene grains from Cr-diopside websterite veins display a similar REE pattern with those from the host peridotites. However, the REE concentrations do not show any consistency. For sample DM-1, the websterite-and peridotite-derived clinopyroxene grains have similar concentrations, whereas in sample 95DA58 the websterite vein clinopyroxene has a lower value than the host peridotite clinopyroxene (Fig. 3B). This observation suggests that the vein might not be the source for the LREE enrichment in the host peridotite. Furthermore, the strongly LREE-enriched pattern of clinopyroxene from anhydrous pyroxenite sample 95DA58 does not completely conform with an origin by crystal fractionation from a basaltic melt, reflecting secondary processes in its history, possibly metasomatic overprinting with LREE-enriched melts (see below).

4.3. Sr, Nd, Pb and Hf isotopic compositions

The Sr, Nd, Pb and Hf isotopic compositions for clinopyroxene separates from the Hannuoba ultramafic xenoliths and the host basalts are listed in Table 3. For comparison with the available data set for the Hannuoba pyroxenite xenoliths (Xu, 2002; Liu et al., 2004), we also determined the whole-rock isotopic composition for a pyroxenite xenolith (95JSB2), which is similar to those studied previously.

Clinopyroxene grains from peridotite have the following isotopic compositions: $^{87}Sr/^{86}Sr = 0.702652–0.704845$, $^{143}Nd/^{144}Nd = 0.512653–0.513216$ ($\varepsilon_{Nd} = +0.3$ to $+11.3$), $^{206}Pb/^{204}Pb = 17.75–19.15$, $^{207}Pb/^{204}Pb = 15.50–15.71$, $^{208}Pb/^{204}Pb = 37.78–39.05$, and $^{176}Hf/^{177}Hf = 0.283038–0.283834$ ($\varepsilon_{Hf} = +9.4$ to $+37.6$). Sr–Nd, Nd–Hf, and Pb–Pb isotopic correlation diagrams are shown in Fig. 4A–D. For comparison, the hypothetical mantle reservoirs of DMM, HIMU (mantle with high U/Pb ratio), EMI and EMII, and the fields for MORB (mid-ocean

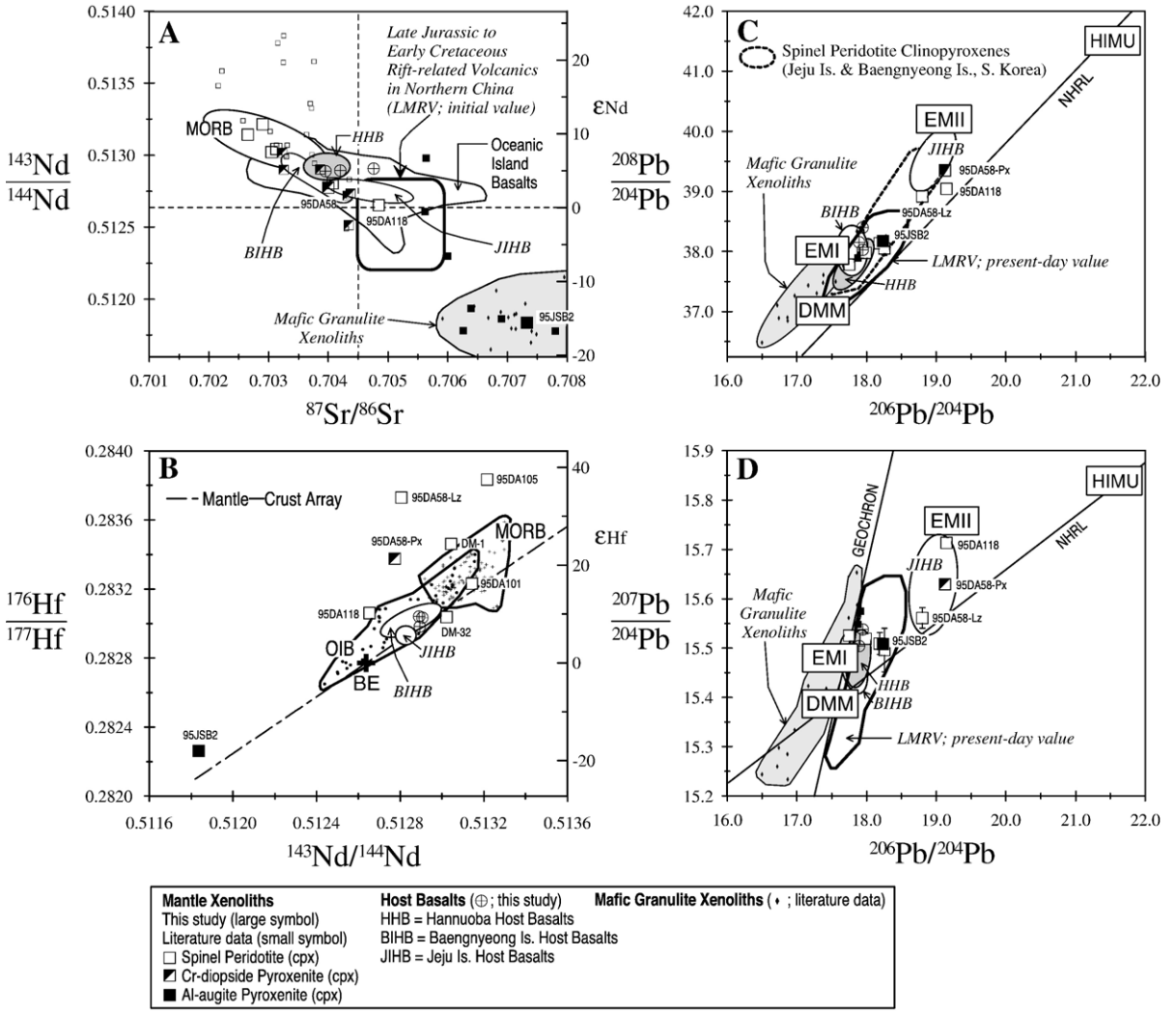

Fig. 4. (A) $^{143}Nd/^{144}Nd$ vs. $^{87}Sr/^{86}Sr$, (B) $^{176}Hf/^{177}Hf$ vs. $^{143}Nd/^{144}Nd$, (C) $^{208}Pb/^{204}Pb$ vs. $^{206}Pb/^{204}Pb$, and (D) $^{207}Pb/^{204}Pb$ vs. $^{206}Pb/^{204}Pb$ isotopic ratios of clinopyroxene separated from the Hannuoba ultramafic xenoliths. Fields for oceanic basalts are from Zindler and Hart (1986), Salters (1996), Salters and White (1998), Chauvel and Blichert-Toft (2001), Andres et al. (2004), Hanan et al. (2004), and Blichert-Toft et al. (2005). Large symbols represent data from this study, and small symbols represent literature data. Data sources: Hannuoba host basalts (Song et al., 1990; Basu et al., 1991), Hannuoba mafic granulite xenoliths (Zhou et al., 2002; Liu et al., 2004), Hannuoba spinel peridotite xenoliths (Song and Frey, 1989; Tatsumoto et al., 1992; Rudnick et al., 2004), Hannuoba pyroxenites xenoliths (Song and Frey, 1989; Tatsumoto et al., 1992; Xu, 2002; Liu et al., 2004), Late Jurassic to Early Cretaceous rift-related volcanic rocks in Northern China (Shao et al., 2001), Korean spinel peridotite xenoliths (Choi et al., 2005), and the basaltic rocks from Baengnyeong Island and Jeju Island, South Korea (Choi et al., 2006a). The bulk Earth $^{176}Hf/^{177}Hf$ value (BE) and the mantle–crust array in the (B) are from Blichert-Toft and Albarède (1997) and Blichert-Toft et al. (1999). Error bars are 2σ uncertainties, and are given only where they exceed the size of the symbol in the plot. Mantle components are from Zindler and Hart (1986): DMM = depleted mantle, EMI and EMII = enriched mantle of type 1 and type 2, respectively, and HIMU = mantle with high U/Pb ratio. The field for MORB (mid-ocean ridge basalt) is shown for comparison. NHRL is the Northern Hemisphere Reference Line of Hart (1984).

ridge basalts) and OIB (oceanic island basalts) are also shown on these diagrams. $^{87}Sr/^{86}Sr$ and $^{143}Nd/^{144}Nd$ ratios for the studied peridotite clinopyroxene extend from the MORB field to the bulk earth value along the Sr–Nd 'mantle array' in Fig. 4A, agreeing with the previously reported isotopic data for clinopyroxene from the Hannuoba peridotite (Song and Frey, 1989; Tatsumoto et al., 1992; Rudnick et al., 2004). The Hf isotopic compositions of all Hannuoba peridotite clinopyroxene samples are depleted relative to the chondritic reservoir (Fig. 4B). We have shown the so-called Nd–Hf 'mantle array' (Vervoort and Blichert-Toft, 1999) in Fig. 4B, but also note that samples 95DA105 and 95DA58 plot well above this array. For the purpose of illustrating the relative size of the Nd–Hf

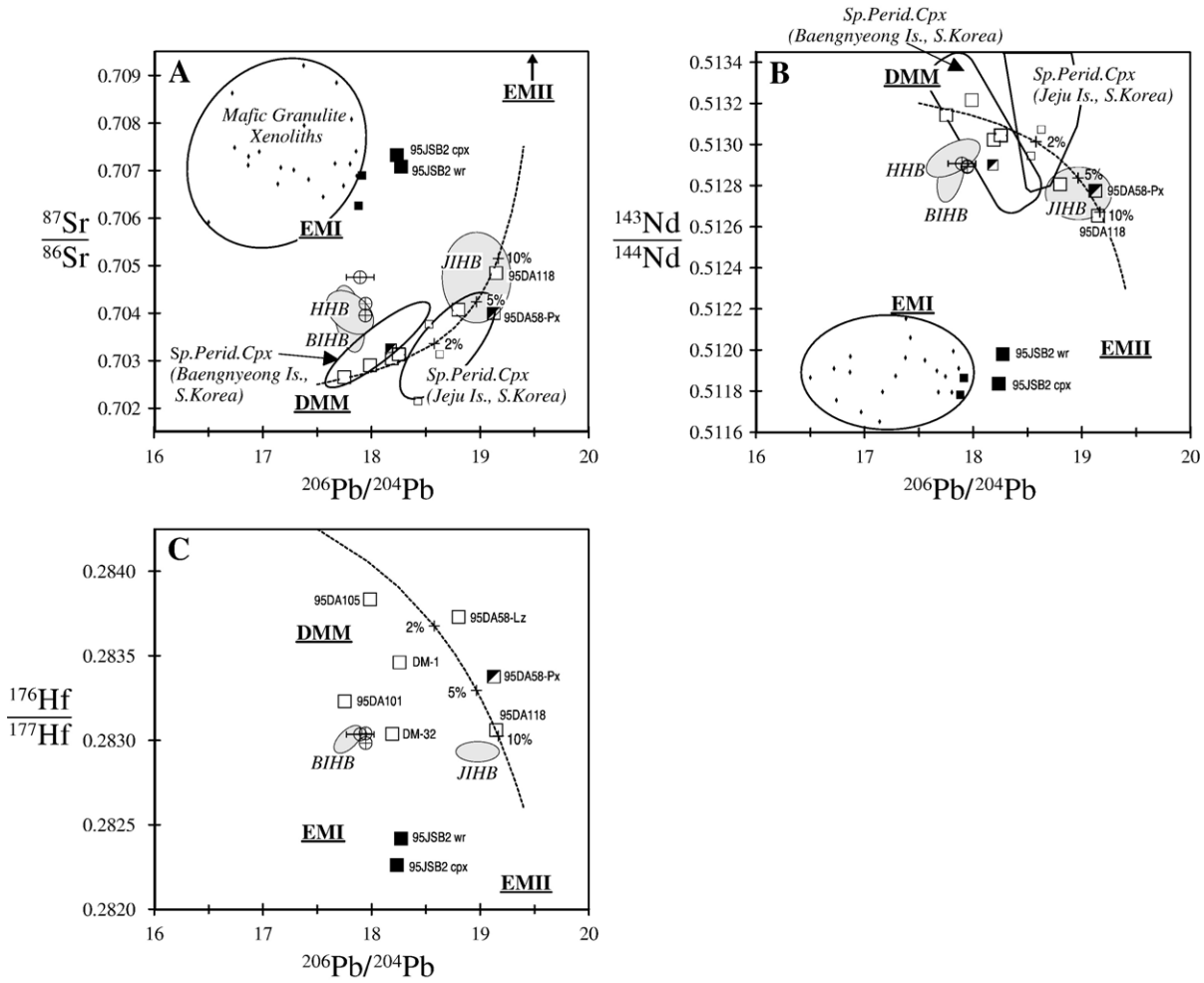

Fig. 5. (A) $^{87}Sr/^{86}Sr$ vs. $^{206}Pb/^{204}Pb$, (B) $^{143}Nd/^{144}Nd$ vs. $^{206}Pb/^{204}Pb$, and (C) $^{176}Hf/^{177}Hf$ vs. $^{206}Pb/^{204}Pb$ isotopic ratios of clinopyroxene separated from the Hannuoba ultramafic xenoliths. All error bars are 2σ uncertainties, and are given only where they exceed the size of the symbol in the plot. Symbols as in Fig. 4. Data sources for mantle components, Hannuoba xenoliths and their host basalts, and Korean spinel peridotite xenoliths and their host basalts are as in Fig. 4. Dashed lines are the calculated binary mixing curves between depleted MORB-like mantle and some inferred, isotopically enriched basaltic melt. Abbreviations: cpx = clinopyroxene, wr = whole-rock.

decoupling observed in the samples, we use the $\Delta\varepsilon_{Hf}$ notation of Beard and Johnson (1993), where $\Delta\varepsilon_{Hf}=\varepsilon_{Hf}-(1.36\ \varepsilon_{Nd}+3.0)$ (Vervoort and Blichert-Toft, 1999). This concept is useful for denoting the magnitude of the deviation from the mantle array. The values of $\Delta\varepsilon_{Hf}$ for the 95DA105 and 95DA58 are +19 and +26, respectively, both significantly high. The Hannuoba clinopyroxene separates exhibit very low values and limited range in $^{176}Lu/^{177}Hf$ ratios (0.030–0.046; Table 3), indicating that these grains are not likely to be the result of sub-solidus breakdown of garnet, which is consistent with their flat HREE patterns (Fig. 3A and B). The Hannuoba peridotite clinopyroxene grains are characterized by a wide range of Pb isotopic compositions, plotting above the northern hemisphere regression line (NHRL) of Hart (1984) (Fig. 4C and D), particularly on the $^{208}Pb/^{204}Pb$ vs. $^{206}Pb/^{204}Pb$ diagram. This reflects a time-integrated record of elevated Th/U, a characteristic known as the DUPAL isotopic signature, prevalent in the Indian Ocean region and some surrounding landmasses.

Clinopyroxene from Cr-diopside websterite vein (95DA58-Px) has a Nd isotopic composition ($^{143}Nd/^{144}Nd=0.512774\pm21$; $\varepsilon_{Nd}=+2.7$) that is within error of the host peridotite clinopyroxene value ($^{143}Nd/^{144}Nd=0.512806\pm19$; $\varepsilon_{Nd}=+3.3$), whereas the Sr, Pb, and especially Hf isotopic compositions ($^{87}Sr/^{86}Sr=0.704001$, $^{206}Pb/^{204}Pb=19.13$, $^{207}Pb/^{204}Pb=15.63$, $^{208}Pb/^{204}Pb=39.35$, $^{176}Hf/^{177}Hf=0.283377$, and $\varepsilon_{Hf}=+21.4$) are significantly different, and in fact, are outside analytical uncertainties when compared to those of the

peridotite wall-rock ($^{87}Sr/^{86}Sr$=0.704074, $^{206}Pb/^{204}Pb$=18.80, $^{207}Pb/^{204}Pb$=15.56, $^{208}Pb/^{204}Pb$=38.92, $^{176}Hf/^{177}Hf$=0.283729, and ε_{Hf}=+33.8). This Cr-diopside websterite sample is characterized by Nd–Hf isotopic decoupling ($\Delta\varepsilon_{Hf}$=+15) (Fig. 4B). The Sr and Nd isotopic compositions are within the field of reported data for the Hannuoba Cr-diopside series pyroxenites (Song and Frey, 1989; Tatsumoto et al., 1992; Xu, 2002), which form a linear trend along the Sr–Nd mantle array, and also overlap with the field for enriched Hannuoba peridotites (Fig. 4A).

Clinopyroxene from Al-augite pyroxenite (95JSB2) is characterized by highly radiogenic Sr, unradiogenic Nd and Hf, and moderate Pb isotopic compositions: $^{87}Sr/^{86}Sr$=0.707327, $^{143}Nd/^{144}Nd$=0.511836 (ε_{Nd}=−15.6), $^{176}Hf/^{177}Hf$=0.282262 (ε_{Hf}=−18.0), $^{206}Pb/^{204}Pb$=18.23, $^{207}Pb/^{204}Pb$=15.51 and $^{208}Pb/^{204}Pb$=38.17. These Sr, Nd and Hf isotopic compositions, along with the previously reported data set for the Hannuoba Al-augite series pyroxenites (Xu, 2002; Liu et al., 2004), plot outside the isotopic compositional range defined by oceanic basalts (Fig. 4A and B). The Nd and Hf isotopic compositions are coupled, plotting along the Nd–Hf 'mantle–crust array' (Fig. 4B). However, we observe small differences in isotopic compositions between the whole-rock and clinopyroxene separate for sample 95JSB2 (Table 3). The whole-rock has less radiogenic $^{87}Sr/^{86}Sr$ and more radiogenic $^{143}Nd/^{144}Nd$ and $^{176}Hf/^{177}Hf$ compared to the clinopyroxene, though the two $^{206}Pb/^{204}Pb$ values are the same within analytical uncertainty.

The host alkali basalts have a limited range of isotopic compositions ($^{87}Sr/^{86}Sr$=0.703954–0.704758, $^{143}Nd/^{144}Nd$=0.512890–0.512907 (ε_{Nd}=+4.9 to +5.2), $^{176}Hf/^{177}Hf$=0.282984–0.283041 (ε_{Hf}=+7.5 to +9.5), $^{206}Pb/^{204}Pb$=17.89–17.95, $^{207}Pb/^{204}Pb$=15.50–15.54, and $^{208}Pb/^{204}Pb$=38.03–38.40), a characteristic in strong contrast with the more varied isotopic compositions of the ultramafic xenoliths. Our results on the host lavas are in good agreement with the earlier Sr–Nd–Pb isotopic data published by Song et al. (1990) and Basu et al. (1991), as shown in Fig. 4A, C and D. Measured for the first time ever for Hannuoba materials, the Hf isotopic compositions reported here are strongly coupled with the Nd isotopic compositions, plotting within the field defined by oceanic island basalts on the Nd–Hf plot (Fig. 4B). The whole-rock compositions of xenolith sample 95JSB2 plot closer to the Hannuoba host basalts than does the clinopyroxene separate on the various isotopic correlation diagrams (Fig. 5A–C), implying that infiltration of the host basalt magma between the grain boundaries during transit to the surface may be responsible for the whole-rock having less radiogenic Sr and more radiogenic Nd and Hf isotopic compositions than the clinopyroxene separate.

5. Discussion

5.1. Mantle source for the host basalt volcanism

The Sr, Nd and Pb isotopic compositions of Late Cenozoic intraplate basalts in East Asia indicate that three different mantle components, i.e., DMM, EMI and EMII, were involved in the magma genesis (Song et al., 1990; Basu et al., 1991; Tatsumoto et al., 1992; Chung et al., 1994, 1995; Hoang et al., 1996; Zhang et al., 1998; Chung, 1999; Zou et al., 2000). Most intriguing about the isotopic characteristics of the basalts is the regional difference in $^{206}Pb/^{204}Pb$ ratios, requiring two large-scale isotopic domains in the mantle source: DMM–EMI for northeast China, and DMM–EMII for Southeast Asia (Liu et al., 1994; Smith, 1998; Chung, 1999; Zou et al., 2000). Choi et al. (2006a) recently reported that the Korean basalts geographically located between these two broad domains show systematic variation from north (Baengnyeong Island, BI in Fig. 1B) to south (Jeju Island, JI in Fig. 1B), with BI basalts defining a DMM–EMI array, whereas the JI basalts yield a DMM–EMII array on various isotopic correlation diagrams.

In order to test whether the lithospheric mantle was the source of magma erupted in East Asia Cenozoic volcanism, the isotopic compositions we have determined for the mantle-derived xenoliths and their host basalts, along with the published data, have been modeled on the $^{87}Sr/^{86}Sr$ vs. $^{206}Pb/^{204}Pb$, $^{143}Nd/^{144}Nd$ vs. $^{206}Pb/^{204}Pb$, and $^{176}Hf/^{177}Hf$ vs. $^{206}Pb/^{204}Pb$ correlation diagrams (Fig. 5A–C), in reference to the mantle end members DMM, EMI, EMII, and HIMU. We have also included on the diagrams the data for two representative Korean basalts (BI and JI) and mantle xenoliths (Choi et al., 2005) hosted by these basalts for comparison.

The Hannuoba host basalts exhibit an array between DMM and EMI on the $^{87}Sr/^{86}Sr$ vs. $^{206}Pb/^{204}Pb$ and $^{143}Nd/^{144}Nd$ vs. $^{206}Pb/^{204}Pb$ correlation diagrams, as discussed in previous studies (Song et al., 1990; Basu et al., 1991; Tatsumoto et al., 1992). Our Hf isotopic compositions plotted against other isotopic systems (e.g., the Pb–Hf diagram in Fig. 5C) also show the DMM–EMI components to be the principal end members. From a geographic point of view, it is of interest to note that the isotopic fields for the Hannuoba basalts overlap with those of the BI basalts (Fig. 1B) on the various isotopic correlation diagrams (Fig. 5A–C).

Unlike the host basalts which define a limited range in $^{206}Pb/^{204}Pb$ ratios, nevertheless implicating EMI or EMII as important end members, the Hannuoba and Korean peridotite clinopyroxene samples cover a wide range in these values (Figs. 4C–D, and 5). Furthermore, the Hannuoba peridotites and Cr-diopside pyroxenites show a mixing hyperbola between DMM and EMII on the $^{87}Sr/^{86}Sr$ vs. $^{206}Pb/^{204}Pb$ and $^{143}Nd/^{144}Nd$ vs. $^{206}Pb/^{204}Pb$ plots (Fig. 5A and B). However, their $^{176}Hf/^{177}Hf$ ratios plotted against $^{206}Pb/^{204}Pb$ ratios do not produce a single array (Fig. 5C). Clinopyroxene from the Korean peridotite xenoliths hosted by both BI and JI basalts also exhibit distinct DMM–EMII arrays on the Sr–Pb and Nd–Pb co-variation diagrams (Fig. 5A and B). Note on these same diagrams that the Hannuoba Al-augite pyroxenites plot outside the isotopic range defined by oceanic basalts, the mixing arrays defined by peridotites/Cr-diopside pyroxenite, and even the host basalt. They are characterized by moderately radiogenic $^{206}Pb/^{204}Pb$ ratios relative to the peridotites/Cr-diopside pyroxenites (Fig. 5A–C). The results show that neither peridotite nor the two types of pyroxenite possesses the characteristic EMI signature for the Hannuoba host basalt source. These observations imply that a genetic relationship between the peridotites/pyroxenites and the Late Cenozoic host volcanism is weak at best. Therefore, we suggest that the asthenospheric mantle is likely to be the most dominant source for the Late Cenozoic intraplate volcanism in East Asia.

5.2. Nature of the metasomatizing agents

On the REE patterns for the Hannuoba peridotite clinopyroxene grains (Fig. 3A–B), we note that samples with relatively high HREE concentrations, such as DM-32 and 95DA101, display LREE-depleted patterns, whereas those with low HREE, such as 95DA58 and 95DA118, have LREE-enriched patterns. These characteristics are not consistent with simple melt extraction, but instead reflect some overprinting by secondary cryptic metasomatism in the history of the xenoliths, as discussed in previous studies of the Hannuoba peridotites (Song and Frey, 1989; Rudnick et al., 2004). Moreover, the relative LREE enrichment is not perfectly correlated with the HREE concentrations. For example, the $(Yb)_N$ of sample 95DA101 is 10.1, which is similar to that of 95DA105 at 9.7. However, the former shows a LREE-depleted pattern, while the latter has a spoon-shaped pattern. In addition, the samples showing LREE-depleted patterns, such as 95DA101, are not as severely depleted in these elements as the Hannuoba sample DM1-9 characterized by Song and Frey (1989), which has similar HREE abundances (Fig. 3A). This suggests that all the studied Hannuoba samples have had their LREE modified to some degree by metasomatic activity. Chromatographic migration of LREE-enriched melts/fluids through LREE-depleted peridotite, involving spatial or temporal evolution of melt volume and composition as a result of melt-rock reaction, has been suggested as a mechanism for generating such variable REE patterns (Navon and Stolper, 1987; Bodinier et al., 1990; Takazawa et al., 1992; Bedini et al., 1997).

The isotopic data obtained for Hannuoba peridotite clinopyroxene are shown in Fig. 6 as a function of the Cr# (expressed as 100Cr/(Cr+Al)) in corresponding spinel. Spinel Cr# is a well known, sensitive indicator of the extents to which the spinel peridotites have lost their basaltic components (Dick and Bullen, 1984). The Sr, Nd and Pb isotopic systematics show, in general, good correlations with the degree of depletion. However, the most depleted sample (95DA118), which has the highest Cr# in spinel, Mg# and Ni concentration in bulk rock, and the lowest HREE concentrations in clinopyroxene among the studied samples (Tables 1 and 2), exhibits the highest $^{87}Sr/^{86}Sr$ and $^{206}Pb/^{204}Pb$, and the lowest $^{143}Nd/^{144}Nd$ ratios. The explanation for this correlation is that the secondary metasomatic overprinting by LREE-enriched melts/fluids involved considerable isotopic variability. The mixing hyperbola between DMM and EMII on the Sr–Pb and Nd–Pb isotopic correlation diagrams (Fig. 5A and B) defined by the Hannuoba clinopyroxene grains suggests that the lithosphere beneath Hannuoba initially had a residual MORB-like isotopic signature, but then was modified by the introduction of metasomatic agents possessing the highly radiogenic EMII signature.

However, a complication arises when the Hf isotopic compositions are considered as illustrated in Fig. 6D. At first, it might seem that there is no correlation between $^{176}Hf/^{177}Hf$ ratios and the degree of depletion. However, the least depleted three samples (DM-32, 95DA101, and 95DA105) define a strong positive correlation with the Cr# in coexisting spinel. Furthermore, their $^{143}Nd/^{144}Nd$ ratios are positively correlated with the Cr# (Fig. 6C), though without the wide spread in isotopic ratios that is observed in the Hf isotopic values. We interpret this characteristic to mean that the second-stage overprinting by metasomatizing agents did not markedly modify the pristine Hf isotopic compositions of the three samples. Their relatively high Hf concentration level (0.7–1.6 ppm, Table 3) might have been the reason why these samples were not so easily reset.

Meanwhile, we observe a negative correlation between $^{176}Hf/^{177}Hf$ and the degree of depletion for the

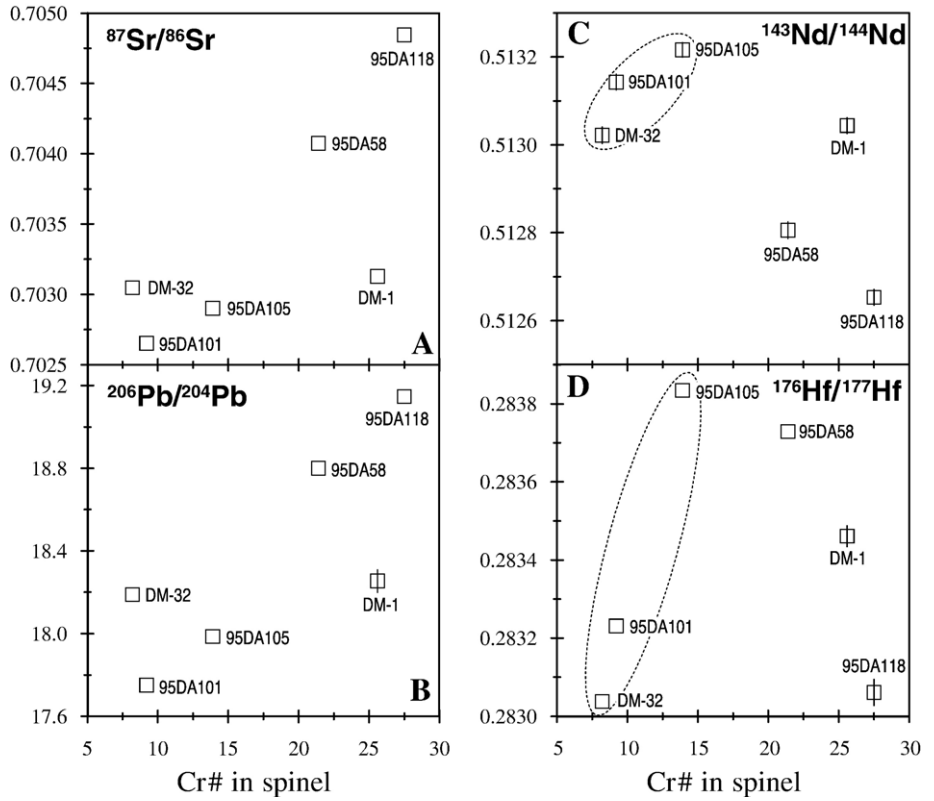

Fig. 6. Sr, Nd, Pb and Hf isotopic compositions of clinopyroxene vs. Cr# (=100Cr/(Cr+Al)) of coexisting spinel from the Hannuoba peridotite xenoliths. All error bars are 2σ uncertainties, and are given only where they exceed the size of the symbol in the plot.

other three samples in Fig. 6D, reflecting what we interpret to be metasomatic overprinting, evidently facilitated by their lower Hf concentrations (0.4–0.5 ppm, Table 3). The most depleted portions of the lithosphere are more susceptible to modification by the metasomatic agents due to their lower bulk distribution coefficients and/or higher permeability (Toramaru and Fujii, 1986; Bedini et al., 1997). We consider silicate melts to be the most likely candidates for this cryptic metasomatism documented in the Hannuoba peridotites.

Alternative candidates such as $CO_2 \pm H_2O$-rich fluids or carbonatite melts, and slab-derived hydrous melts are ruled out because hydrous arc and carbonatitic magmas are characterized by strong depletions in Nb and Ta relative to the large-ion lithophile elements (LILE) such as K, Rb, Ba, U and Th (e.g., McCulloch and Gamble 1991; Bizimis et al., 2003b), and overall, low concentrations of all the high field strength elements (HFSE) — Nb, Ta, Zr, Hf, and Ti. For example, average Hf concentration in carbonatite is 0.6 ppm (Bizimis et al., 2003b), which is significantly lower than typical values for oceanic island basalts (7.8 ppm; Sun and McDonough, 1989). Woodhead et al. (2001) reported mean Hf concentrations for Mariana and New Britain arc basalts of 1.4 and 1.1 ppm, respectively. Therefore, the other agents do not carry a significant amount of Hf without appreciable changes to their major oxide concentrations. The absence of hydrous minerals (including apatite) and/or secondary clinopyroxene in our sample suite of Hannuoba peridotite and pyroxenite further support silicate melts as the metasomatic agents. Simple binary mixing calculations show that addition of up to ~10% of average oceanic basaltic melts (Sr=660 ppm; Nd=38.5 ppm, Pb=3.2 ppm, Hf=7.8 ppm; Sun and McDonough, 1989) of radiogenically enriched EMII-like isotopic composition to a DMM-dominated mantle lithosphere clinopyroxene (Sr=65 ppm; Nd=3 ppm, Pb=0.05 ppm, Hf=0.3 ppm) can account for the isotopic signatures observed in the Hannuoba peridotite clinopyroxene separates (Fig. 5A–C).

Hannuoba Cr-diopside pyroxenite sample 95DA58-px and some literature data plot along the mixing hyperbola defined by peridotite clinopyroxene on the Sr–Pb, Nd–Pb and Hf–Pb isotopic diagrams (Fig. 5A–C). However, the metasomatizing agent overprinting the EMII-like signature is not likely to be cogenetic with the parental melts of Cr-diopside pyroxenite, based on two observations

explained immediately below. First, the pyroxenite samples do not possess the most isotopically enriched signatures in the studied suite. For example, peridotite sample 95DA118 is isotopically more enriched than the pyroxenite samples. Furthermore, we observe the secondary metasomatic overprinting history preserved even in the pyroxenite samples, such as the LREE-enrichment of clinopyroxene in sample 95DA58-px. In Fig. 3D, we have shown the REE pattern of an estimated equilibrium melt with 95DA58-px clinopyroxene. Four different sets of partition coefficients published by Hart and Dunn (1993), Hauri et al. (1994), and Green et al. (2000) for experimental runs at 1380°/3.0 GPa, 1430°/2.5 GPa, 1405°/1.7 GPa and 1080°/2.0 GPa, respectively, have been adapted in the calculations.

The calculated REE patterns have been compared with data for host alkali basalts as well as Hannuoba tholeiites (Liu et al., 1994). The Hannuoba pyroxenites are considered to be crystal segregates formed by a flow crystallization process in magma conduits (Xu, 2002), as proposed by several authors for pyroxenite bands and veins in high-temperature peridotite bodies and ultramafic xenoliths (e.g., Bodinier et al. 1988, 1990; Mukasa and Shervais 1999). We note that the melt equilibrated with the 95DA58-px had been uncommonly enriched in LREEs relative to HREEs, which is not reconciled with realistic crystal/melt equilibria; even in consideration of the large uncertainties for this type of calculation, such as (1) the dependence of partition coefficients on P–T–X–f_{O_2} conditions, and (2) our usage of partition coefficients determined for magmatic phases. Furthermore, the observation of decoupling between Nd and Hf isotopic compositions of the sample (Fig. 4B) independently supports our interpretation for the secondary events.

The EMII-like signature observed in the Hannuoba peridotites/Cr-diopside pyroxenites is strongly different from the Al-augite series pyroxenites characterized by moderately radiogenic Pb isotopic compositions (Fig. 5A–C), which rules out the notion that the melt which produced the vein also produced the metasomatism. As well, the peridotites/Cr-diopside pyroxenites cannot be the source of parental magmas for the Al-augite pyroxenites because of the significant differences in isotopic ratios between the two types of pyroxenite, requiring origination in two separate melting events.

5.3. The Neoarchean Lu–Hf isochron age for the Hannuoba peridotites

The $^{147}Sm/^{144}Nd$ and $^{143}Nd/^{144}Nd$ ratios of Hannuoba peridotite clinopyroxene separates produced by this study combined with previously published data by Song and Frey (1989), Tatsumoto et al. (1992), and Rudnick et al. (2004), range from subchondritic to superchondritic, and form a positive trend on a Sm–Nd isochron diagram (Fig. 7A). This trend has too much scatter to have chronologic significance, but coincides remarkably well with the 2.7 Ga isochron for the Huai'an terrain granulites in the Trans-North China Orogen (Liu et al., 2004) (Fig. 1 for the location). The Nd model ages for the individual data points are variable, from ~2.8 Ga to negative ages (Table 3), consistent with our earlier observation that REE patterns for all the samples display some degree of secondary metasomatic overprinting by LREE-enriched silicate melts. The Sm–Nd isotopic systematics seem to have been modified extensively by the interaction.

In contrast, the $^{176}Lu/^{177}Hf$ and $^{176}Hf/^{177}Hf$ ratios of the Hannuoba peridotite clinopyroxene separates are mostly superchondritic (Fig. 7B), and three of them (DM-32, 95DA101, and 95DA105) still contain Hf isotopic characteristics consistent with minimal metasomatic overprinting of residues produced by the last major melt extraction event (see above). These three samples define a Lu–Hf isochron age of 2.59±0.09 Ga (2σ) (MSWD=0.18) with an initial $^{176}Hf/^{177}Hf$ ratio of 0.281551 (ε_{Hf}=+15; Fig. 7B) when the $\lambda^{176}Lu$ value of 1.865×10^{-11} year^{-1} (Scherer et al., 2001) is used in the calculation. We interpret this Neoarchean age to mark the time of stabilization of the mantle section by melt extraction, which is supported by the positive initial ε_{Hf} value of +15. The Sm–Nd isochron crystallization age of 2.7±0.4 Ga (2σ) estimated for the nearby Huai'an terrain igneous granulites (Liu et al., 2004), as shown in Fig. 7A, provides additional support for the Neoarchean events in the development of the depleted character of the Hannuoba peridotites. Furthermore, Wilde et al. (2006) reported SHRIMP U–Pb ages for zircons extracted from some Hannuoba peridotite xenoliths ranging from 2.6 to 1.8 Ga. These lines of evidence suggest that stabilization of the lithospheric mantle beneath Hannuoba was contemporaneous with formation of the overlying crust.

Recently, Pearson and Nowell (2003) showed that clinopyroxene in a suite of peridotite samples from Beni Bousera massif, northern Morocco, define a Lu–Hf isochron of 1.43±0.07 Ga (2σ), which is within error of the most reliable Re–Os model age ca. 1.2–1.4 Ga for the peridotite massif. They argued that the Lu–Hf system shows potential to improve constraints on the timing of lithospheric mantle differentiation. Furthermore, in a study of peridotite xenoliths from the Homestead kimberlites of the Wyoming Craton, Carlson et al. (2004) also showed that the Lu–Hf system in some of the peridotites

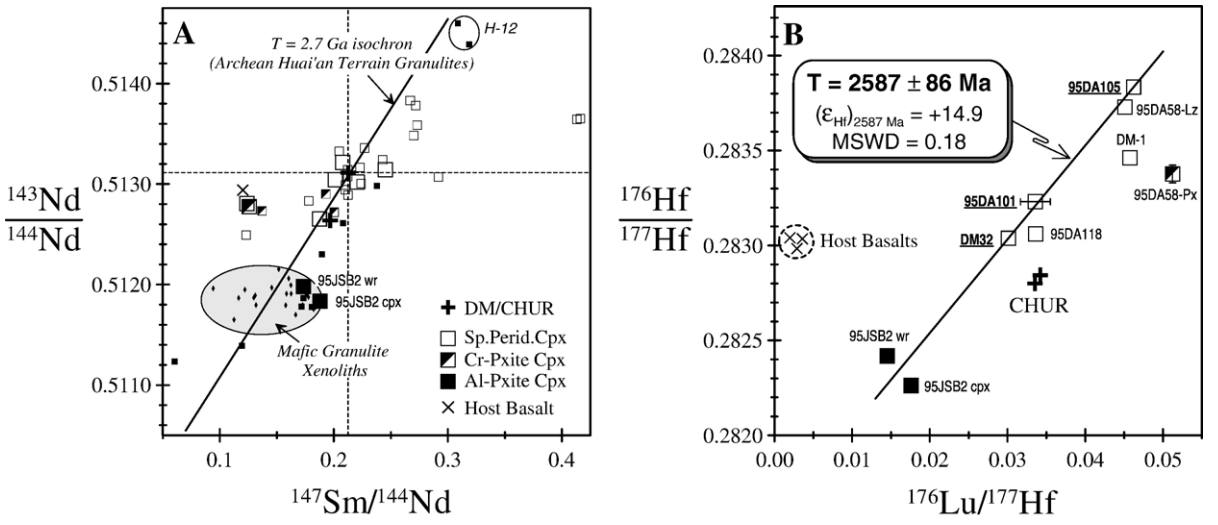

Fig. 7. (A) $^{143}Nd/^{144}Nd$ vs. $^{147}Sm/^{144}Nd$, and (B) $^{176}Hf/^{177}Hf$ vs. $^{176}Lu/^{177}Hf$ ratios for clinopyroxene separated from the Hannuoba ultramafic xenoliths. Sm–Nd data sources for the Hannuoba xenoliths are as in Fig. 4. The Sm–Nd isochron for the Huai'an terrain granulites of igneous affinities (Liu et al., 2004) is shown for comparison. All error bars are 2σ uncertainties, and are given only where they exceed the size of the symbol in the plot. The solid line in (B) is an isochron for the samples underlined. Calculation of the Lu–Hf isochron is based on the decay constant $\lambda^{176}Lu = 1.865 \times 10^{-11}$ year^{-1} (Scherer et al., 2001). The present-day CHUR parameters in (B) are from Blichert-Toft and Albarède (1997), Salters and White (1998), and Patchett et al. (2004).

carries memory of the depletion event recorded by the major element composition and Re–Os isotopic system of the samples. For the Hannuoba locality, our data show that the Lu–Hf system can be used to constrain the formation age of the lithospheric mantle. The blocking temperature for the Lu–Hf method is known to be higher than that for Sm–Nd in studies of garnet-bearing, high-grade metamorphic rocks and ultramafic pyroxenite suites (e.g., Blichert-Toft et al., 1999; Scherer et al., 2000; Pearson and Nowell, 2004). Application of the two-pyroxene thermometer of Wells (1977), estimated to have a reproducibility of ±70 °C, yields ~950 °C for the three Hannuoba peridotites (Table 2). This observation suggests that the closure temperature for Lu and Hf diffusion in diopside of anhydrous spinel peridotites might be of the order of ~900 °C.

Peridotite sample DM-32, which has an LREE-depleted pattern (Fig. 3A), exhibits coupled Nd and Hf isotopic compositions (Fig. 4B). Sample 95DA105, showing a spoon-shaped REE pattern (Fig. 3A), however, displays significant Nd–Hf isotopic decoupling, with $\Delta\varepsilon_{Hf}$=+19.2 (Fig. 4B). Peridotite sample 95DA58 has an LREE-enriched pattern (Fig. 3B) and is characterized by even bigger decoupling ($\Delta\varepsilon_{Hf}$=+26.4) compared to sample 95DA105. We interpret the decoupling observed in some samples to be the result of secondary metasomatism severely impacting the Sm–Nd system, but not the more robust Lu–Hf system. Bizimis et al. (2003a,b) have shown that recent metasomatism of an ancient depleted peridotite through melt–peridotite interaction can produce Nd–Hf decoupling, similar to that seen in the Hannuoba peridotites.

Several of the diagrams in Fig. 2 illustrate the compositional ranges of peridotites (mostly garnet harzburgites) hosted in kimberlites erupted through some Archean cratons: Kaapvaal in southern Africa (Boyd, 1989), Udachnaya in Siberia (Griffin et al., 1999), and Slave in Canada (Griffin et al., 1999). Meso-to Neoarchean Re depletion model ages have been reported for these peridotites (Pearson et al., 1995a,b; Irvine et al., 1999). The Hannuoba peridotites are compositionally distinct from the highly refractory (i.e., depleted in magmaphile constituents such as Al_2O_3 and CaO) mantle lithosphere that characterizes the Archean cratons (cf. Rudnick et al., 2004). That is, Hannuoba peridotites are more fertile than typical cratonic peridotites, and judging from garnet paucity, were derived from shallower levels within the mantle. If our Lu–Hf isochron age is robust, then this raises the question of how representative the Archean lithospheric mantle (LM), characterized by strong depletion in magmaphile elements, truly is. Lee et al. (2001) reported some unusually fertile Neoarchean LM beneath Mojavia province, southwestern USA, and proposed the possibility of such fertile Archean LM being overlooked and mistaken for Phanerozoic material.

On the other hand, Gao et al. (2002) reported a Re–Os 'errorchron' age of 1.9±0.2 Ga for the Hannuoba peridotites, based on a regression line forced through primitive upper mantle (PUM), a hypothetical reservoir that has never experienced melt depletion or enrichment (Meisel et al., 2001). However, Walker et al. (2002) raised the question of the true value for PUM. In addition, there is large uncertainty regarding the $^{187}Os/^{188}Os$ evolution of the mantle source for lithospheric peridotites owing to the large range in Os isotopic compositions for the oceanic mantle as sampled by abyssal peridotites (e.g., Snow and Reisberg, 1995; Rudnick and Lee, 2002; Walker et al., 2002). Furthermore, the trend defined by Hannuoba peridotites yielding a ~1.9 Ga Re–Os errorchron age does not pass through the hypothetical PUM composition on the $^{187}Os/^{188}Os$ vs. Al_2O_3 correlation diagram (Table 1; Gao et al., 2002), indicating that it is not simply the result of melt extraction from the primitive mantle.

Interestingly, Gao et al. (2002) showed that the Hannuoba peridotites yield a Re–Os errorchron age of 2.1±0.5 Ga, without forcing the trend through the PUM reservoir. Unequivocally, then, both Os and Hf isotope systematics point to Neoarchean age of depletion. Therefore, the Re–Os systematics of the Hannuoba peridotites might define a chronologically meaningful Neoarchean isochron, if samples compromised by secondary metasomatic overprinting are recognized and excluded from the regression.

In summary, our data confirm that ancient Neoarchean lithospheric mantle persists beneath Hannuoba despite the protracted tectono-magmatic reactivation during the Mesozoic and Cenozoic (e.g., Zhou and Armstrong, 1982; Meng, 2003; Yang et al., 2003; Zhang, 2005). This observation suggests that it is unlikely for the lithospheric mantle in East Asia to have been removed by wholesale delamination. The model of mechanical reactivation of endogenous lithospheric mantle, commonly invoked for the enriched mantle source of the volcanism in East Asia, may need to be reconsidered before we can fully understand mantle dynamics for this region.

5.4. Petrogenetic relationships between the Hannuoba pyroxenites and Late Mesozoic magmatism in Northern China

Pyroxenite and lower crustal granulite (dominantly mafic to intermediate) present in the Hannuoba xenolith suite have been interpreted as cumulates extracted from veins and underplated layers at the crust–mantle boundary, genetically related to Late Jurassic to Early Cretaceous rift-related volcanism in northern China (Xu, 2002; Liu et al., 2001, 2004; Meng, 2003). This view is based largely on the observation that zircon U–Pb ages determined for these xenoliths are the same as the Late Mesozoic eruption ages for the lavas (Fan et al., 1998; Liu et al., 2004). However, Wilde et al. (2003, 2006) argued that some of the mafic granulite xenoliths are likely to be remnants of Precambrian crust based on the ubiquitous presence and locally abundant Precambrian zircons in the xenoliths.

For comparison, we have plotted published Sr, Nd and Pb isotopic compositions for the Hannuoba mafic granulites (Zhou et al., 2002; Liu et al., 2004), Late Mesozoic (~150 to 120 Ma) rift-related lavas in northern China (Shao et al., 2001) and Hannuoba whole-rock Al-augite pyroxenites (Xu, 2002; Liu et al., 2004) along with ours, in Figs. 4, 5 and 7. Note that present-day isotopic values for the pyroxenites and granulites have been plotted on these diagrams (Figs. 4, 5 and 7), and corrected values using a reference age of 150 Ma are given in Table 3. The corrections for a formation age at 150 Ma do not have any impact on the conclusions we reach below because of the very low Rb/Sr, Sm/Nd, Lu/Hf and U/Pb ratios in these samples (Table 3; Xu, 2002; Zhou et al., 2002). The same is true of the small difference in isotopic compositions between whole-rock and the constituent clinopyroxene in the pyroxenite xenoliths.

The Late Mesozoic volcanic rocks are characterized by moderately radiogenic Sr and Nd isotopic compositions — initial $^{87}Sr/^{86}Sr$ ratios of 0.7045 to 0.7059 and $\varepsilon_{Nd}(t)$ values of −8.47 to +3.88 (Shao et al., 2001) (Fig. 4A). Al-augite pyroxenites have Sr and Nd isotopic compositions that fall between and also partly overlap with the fields for Late Mesozoic lavas and the granulite xenoliths (Fig. 4A), with moderately radiogenic Pb isotopic compositions (Fig. 5A and B) plotting to the right of the geochron (Fig. 4D). Therefore, the isotopic characteristics of the Al-augite pyroxenites, as well as the protolith for the mafic granulites, cannot be explained by simple kinship to the Late Mesozoic lavas.

The Al-augite pyroxenites have Sr–Nd–Hf isotopic compositions that do not overlap with the field for oceanic basalts (Fig. 4A and B), which reflect long-term isolation from the convective mantle. Interestingly, the pyroxenites show a positive correlation on the Sm–Nd isochron plot (Fig. 7A), nearly parallel to the Huai'an terrain granulite isochron of ~2.7 Ga. Sample H-12 in Fig. 7A, characterized by superchondritic Sm–Nd systematics and an ε_{Nd} value of ~ +38 (Xu, 2002), leaves no doubt as to its Precambrian origin, as discussed by Xu (2002). One possible interpretation is that the Al-augite pyroxenite xenoliths might be

products of Precambrian magmatism. Recent discovery of Precambrian zircons in the Hannuoba Al-augite pyroxenite xenoliths (Liu et al., 2004) supports this conclusion. Xu (2002) interpreted the positive correlation of these xenoliths on the Sm–Nd isochron as a likely mixing array, and suggested that it is the product of delaminated lower crustal materials mixing with a mantle source that had enriched isotopic components during the Mesozoic magmatic event represented by lavas in the area. Work we have reported here, however, such as ample evidence for preservation of Neoarchean lithospheric mantle beneath Hannuoba (see above), makes it unlikely that wholesale lower crustal delamination occurred.

The Cr-diopside pyroxenite xenoliths plot along a horizontal array on the Sm–Nd isochron diagram (Fig. 7A), but no age information is apparent. Instead, the array is probably due to recent addition of Sm or Nd and concomitant isotopic re-equilibration. On the Lu–Hf isochron plot (Fig. 7B), the Al-augite pyroxenite shows subchondritic Lu–Hf systematics, which is consistent with origination by crystallization from a melt. On the other hand, Cr-diopside pyroxenite (95DA58-px) displays superchondritic $^{176}Lu/^{177}Hf$ and $^{176}Hf/^{177}Hf$ ratios, requiring second-stage evolution, which most probably involved secondary partial melting and melt extraction after emplacement as veins. We can deduce that the secondary partial melting event depleted the rocks in basaltic components and made them susceptible to the subsequent metasomatism recognized from the uncommonly enriched LREEs relative to HREEs (Fig. 3D), and Nd–Hf decoupling (Fig. 4B). Lead isotopic data of Shao et al. (2001) for the Late Mesozoic lavas reproduced in Fig. 4C and D, do not possess the radiogenic EMII-like Pb isotopic signature observed in the Hannuoba Cr-diopside pyroxenite and peridotite xenoliths. This means that the Late Mesozoic magmatism cannot be the metasomatising agent that imprinted the EMII-like signature in the xenoliths. However, it remains an open question whether the parental magmas for the Cr-diopside pyroxenite were cogenetic with the Late Mesozoic magmatism, before the secondary overprinting events.

For a Cr-diopside websterite (95DA58-px), occurring as a composite xenolith, the Nd and Sr isotopic compositions of the websterite are close to those of the host peridotite, whereas their Pb and Hf isotopic compositions are dissimilar. Considering the relative diffusion coefficients in diopside at ~1000 °C — Sr≥Pb>Nd (Sneeringer et al., 1984; Van Orman et al., 2001), and possibly >>Hf, we interpret the coincidence of the Nd isotopic compositions between the two lithologies to be fortuitous. Based on the LREE zoning observed in some clinopyroxene grains from Hannuoba peridotites, and a lack of correlation between Rb/Sr and $^{87}Sr/^{86}Sr$, Song and Frey (1989) and Rudnick et al. (2004) argued in favor of relatively recent metasomatism, possibly during the Cenozoic. This suggestion is consistent with the isotopic disequilibrium we have documented between the Cr-diopside pyroxenite vein and the host peridotite.

6. Conclusions

The main points of the discussion above may be summarized as follows:

(1) The EMI and EMII mantle end members for the mantle source of Late Cenozoic intraplate volcanism in East Asia are not located in the mantle lithosphere.
(2) The mantle lithosphere (spinel peridotites/pyroxenites) is not likely to have been the source of the basaltic magmas making up the Hannuoba volcanic field of the North China Block.
(3) The Cr-diopside xenolith suite exhibits mixing hyperbolas between DMM and EMII, which contrasts with the host Hannuoba basalts produced by mixing components from DMM and EMI. This also means that the Al-augite and Cr-diopside suites are not cogenetic.
(4) Metasomatizing agents – possibly silicate melts – imprinting xenoliths with the EMII-like signature are not likely to be cogenetic with the parental melts of the Cr-diopside pyroxenite, judging from the multi-stage evolutionary history, including secondary partial melting and metasomatic overprinting of the Cr-diopside pyroxenite itself.
(5) Late Mesozoic volcanic rocks in northern China are isotopically different from the Hannuoba peridotites/pyroxenites, ruling out the possibilities of their origin as cogenetic or metasomatic agents.
(6) Evidence for metasomatism is common in the xenolith suites; however, the Hf isotopic signatures are the least affected, which implies that the Lu–Hf system can be used to date mantle melting events as recorded by the peridotite xenolith samples.
(7) The Lu–Hf isochron age of ~2.6 Ga for the largely unmetasomatized Hannuoba peridotites indicates that stabilization of the mantle lithosphere was contemporaneous with formation of the overlying crust, and persisted despite protracted tectonomagmatic reactivation in this area during the Mesozoic and Cenozoic.

Acknowledgements

We thank Bernard Bourdon, and two anonymous reviewers for the constructive reviews that greatly improved the original manuscript. We also thank Tom Vogel and Lina Patiño for the help with the XRF and ICP-MS analyses, and Nobu Shimizu for the assistance with the ion microprobe analyses. This work was supported by the National Science Foundation grants EAR-0207830 and EAR-0440238 to SBM, Korea Polar Research Institute Projects PE07020 and PE07140 to SHC, and National Natural Science Foundation of China grant 40334043 to XHZ.

References

Andres, M., Blichert-Toft, J., Schilling, J., 2004. Nature of the depleted upper mantle beneath the Atlantic: evidence from Hf isotopes in normal mid-ocean ridge basalts from 79°N to 55°S. Earth Planet. Sci. Lett. 225, 89–103.

Basu, A.R., Junwen, W., Wangkang, H., Guanghong, X., Tatsumoto, M., 1991. Major element, REE, and Pb, Nd and Sr isotopic geochemistry of Cenozoic volcanic rocks of eastern China: implications for their origin from suboceanic-type mantle reservoirs. Earth Planet. Sci. Lett. 105, 149–169.

Beard, B.L., Johnson, C.M., 1993. Hf isotope composition of late Cenozoic basaltic rocks from northwestern Colorado, USA: new constraints on mantle enrichment processes. Earth Planet. Sci. Lett. 119, 495–509.

Bedini, R.M., Bodinier, J.-L., Dautria, J.-M., Morten, L., 1997. Evolution of LILE-enriched small melt fractions in the lithospheric mantle: a case study from the East African Rift. Earth Planet. Sci. Lett. 153, 67–83.

Bizimis, M., Sen, G., Salters, V.J.M., 2003a. Hf−Nd isotope decoupling in the oceanic lithosphere: constraints from spinel peridotites from Oahu, Hawaii. Earth Planet. Sci. Lett. 217, 43–58.

Bizimis, M., Salters, V.J.M., Dawson, J.B., 2003b. The brevity of carbonatite sources in the mantle: evidence from Hf isotopes. Contrib. Mineral. Petrol. 145, 281–300.

Bizimis, M., Griselin, M., Lassiter, J.C., Salters, V.J.M., Sen, G., 2007. Ancient recycled mantle lithosphere in the Hawaiian plume: osmium–hafnium isotopic evidence from peridotite mantle xenoliths. Earth Planet. Sci. Lett. 257, 259–273.

Blichert-Toft, J., Albarède, F., 1997. The Lu−Hf isotope geochemistry of chondrites and the evolution of the mantle−crust system. Earth Planet. Sci. Lett. 148, 243–258.

Blichert-Toft, J., Albarède, F., Kornprobst, J., 1999. Lu−Hf isotope systematics of garnet pyroxenites from Beni Bousera, Morocco: implications for basalt origin. Science 283, 1303–1306.

Blichert-Toft, J., Agranier, A., Andres, M., Kingsley, R., Schilling, J., Albarède, F., 2005. Geochemical segmentation of the Mid-Atlantic Ridge north of Iceland and ridge-hot spot interaction in the North Atlantic. Geochem. Geophys. Geosys. 6, 1–27.

Bodinier, J.-L., Dupuy, C., Dostal, J., 1988. Geochemistry of petrogenesis of Eastern Pyrenean peridotites. Geochim. Cosmochim. Acta 52, 2893–2907.

Bodinier, J.-L., Vasseur, G., Vernieres, J., Dupuy, C., Fabries, J., 1990. Mechanism of mantle metasomatism: geochemical evidence from the Lherz orogenic peridotite. J. Petrol. 31, 597–628.

Boyd, F.R., 1989. Compositional distinction between oceanic and cratonic lithosphere. Earth Planet. Sci. Lett. 96, 15–26.

Carlson, R.W., Irving, A.J., Schulze, D.J., Hearn Jr., B.C., 2004. Timing of Precambrian melt depletion and Phanerozoic refertilization events in the lithospheric mantle of the Wyoming Craton and adjacent Central Plains Orogen. Lithos 77, 453–472.

Chauvel, C., Blichert-Toft, J., 2001. A hafnium isotope and trace element perspective on melting of the depleted mantle. Earth Planet. Sci. Lett. 190, 137–151.

Chen, S., O'Reilly, S.Y., Zhou, X., Griffin, W.L., Zhang, G., Sun, M., Feng, J., Zhang, M., 2001. Thermal and petrological structure of the lithosphere beneath Hannuoba, Sino-Korean Craton, China: evidence from xenoliths. Lithos 56, 267–301.

Choi, S.H., Kwon, S.-T., Mukasa, S.B., Sagong, H., 2005. Sr−Nd−Pb isotope and trace element systematics of mantle xenoliths from Late Cenozoic alkaline lavas, South Korea. Chem. Geol. 221, 40–64.

Choi, S.H., Mukasa, S.B., Kwon, S.-T., Andronikov, A.V., 2006a. Sr, Nd, Pb and Hf isotopic compositions of late Cenozoic alkali basalts in South Korea: evidence for mixing between the two dominant asthenospheric mantle domains beneath East Asia. Chem. Geol. 232, 134–151.

Choi, S.H., Mukasa, S.B., Andronikov, A.V., Osanai, Y., Harley, S.L., Kelly, N.M., 2006b. Lu−Hf systematics of the ultra-high temperature Napier metamorphic complex in Antarctica: evidence for the early Archean differentiation of Earth's mantle. Earth and Planet. Sci. Lett. 246, 305–316.

Chung, S.-L., 1999. Trace element and isotope characteristics of Cenozoic basalts around the Tanlu Fault with implications for the eastern plate boundary between North and South China. J. Geol. 107, 301–312.

Chung, S.-L., Sun, S., Tu, K., Chen, C.-H., Lee, C., 1994. Late Cenozoic basaltic volcanism around the Taiwan Strait, SE China: product of lithosphere–asthenosphere interaction during continental extension. Chem. Geol. 112, 1–20.

Chung, S.-L., Jahn, B.-M., Chen, S.-J., Lee, T., Chen, C.-H., 1995. Miocene basalts in northwestern Taiwan: evidence for EM-type mantle sources in the continental lithosphere. Geochim. Cosmochim. Acta 59, 549–555.

Dick, H.J.B., Bullen, T., 1984. Chromian spinel as a petrogenetic indicator in abyssal and alpine-type peridotites and spatially associated lavas. Contrib. Mineral. Petrol. 86, 54–76.

Fan, Q., Liu, R., Li, N., Sui, J., Lin, Z., 1998. Zircon chronology and REE geochemistry of granulite xenoliths at Hannuoba. Chin. Sci. Bull. 43, 1510–1515.

Fan, W.M., Zhang, H.F., Baker, J., Jarvis, K.E., Mason, P.R.D., Menzies, A., 2000. On and off the North China Craton: where is the Archean keel? J. Petrol. 41, 933–950.

Frey, F.A., Prinz, M., 1978. Ultramafic inclusions from San Carlos, Arizona: petrologic and geochemical data bearing on their petrogenesis. Earth Planet. Sci. Lett. 38, 129–176.

Gao, S., Rudnick, R.L., Carlson, R.W., McDonough, W.F., Liu, Y., 2002. Re−Os evidence for replacement of ancient mantle lithosphere beneath the North China Craton. Earth Planet. Sci. Lett. 198, 307–322.

Green, T.H., Blundy, J.D., Adam, J., Yaxley, G.M., 2000. SIMS determination of trace element partition coefficients between garnet, clinopyroxene and hydrous basaltic liquids at 2−7.5 GPa and 1080−1200 °C. Lithos 53, 165–187.

Griffin, W.L., Zhang, A.D., O'Reilly, S.Y., Ryan, C.G., 1998. Phanerozoic evolution of the lithosphere beneath the Sino-Korean craton. In: Flower, M., Chung, S.-L., Lo, C.-H., Lee, T.-Y. (Eds.), Mantle Dynamics and Plate Interactions in East Asia. Am. Geophys. Union, Geophys. Monogr., vol. 27, pp. 107–126.

Griffin, W.L., O'Reilly, S.Y., Ryan, C.G., 1999. The composition and origin of sub-continental lithospheric mantle. In: Fei, Y., Bertka, M., Mysen, B.O. (Eds.), Mantle Petrology; Field Observation and High Pressure Experimentation—A Tribute to Francis R. (Joe) Boyd. Geochem. Soc. Spec. Publ., vol. 6, pp. 13–45.

Hannah, R.S., Vogel, T.A., Patino, L.C., Alvarado, G.E., Perez, W., Smith, D.R., 2002. Origin of silicic volcanic rocks in Central Costa Rica: a study of a chemically variable ash-flow sheet in the Tiribi Tuff. Bull. Volcan. 64, 117–133.

Hanan, B.B., Blichert-Toft, J., Pyle, D.G., Christie, D.M., 2004. Contrasting origins of the upper mantle revealed by hafnium and lead isotopes from the Southeast Indian Ridge. Nature 432, 91–94.

Hart, S.R., 1984. A large-scale isotope anomaly in the southern hemisphere mantle. Nature 309, 753–757.

Hart, S.R., Dunn, T., 1993. Experimental cpx/melt partitioning of 24 trace elements. Contrib. Mineral. Petrol. 113, 1–8.

Hauri, E.H., Wagner, T.P., Grove, T.L., 1994. Experimental and natural partitioning of Th, U, Pb and other trace elements between garnet, clinopyroxene and basaltic melts. Chem. Geol. 117, 149–166.

Hoang, N., Flower, M., Carlson, R.W., 1996. Major, trace, and isotopic compositions of Vietnamese basalts: interaction of hydrous EM1-rich asthenosphere with thinned Eurasian lithosphere. Geochim. Cosmochim. Acta 60, 4329–4351.

Irvine, G.J., Kopylova, M.G., Carlson, R.W., Pearson, D.G., Shirey, S.B., Kjarsgaard, B.A., 1999. Age of the lithospheric mantle beneath and around the Slave craton: a Re−Os isotope study of peridotite xenoliths from the Jericho and Somerset island kimberlites. 9th Annual V.M. Goldschimidt Conference, August 22–27, 1999, Cambridge, Massachusetts. abstract no. 7229.

Irving, A.J., Frey, F.A., 1978. Distribution of trace elements between garnet megacrysts and host volcanic liquids of kimberlitic to rhyolitic composition. Geochim. Cosmochim. Acta 42, 771–787.

Irving, A.J., Frey, F.A., 1984. Trace element abundances in megacrysts and their host basalts: constraints on partition coefficients and megacryst genesis. Geochim. Cosmochim. Acta 48, 1201–1221.

Kern, H., Gao, S., Liu, Q.-S., 1996. Seismic properties and densities of middle and lower crustal rocks exposed along the North China Geoscience Transect. Earth Planet. Sci. Lett. 139, 439–455.

Kröner, A., Composton, W., Zhang, G.W., Guo, A.L., Todt, W., 1988. Ages and tectonic setting of Late Archean greenstone-gneiss terrain in Henan Province, China as revealed by single-grain zircon dating. Geology 16, 211–215.

Lee, C.-T., Yin, Q., Rudnick, R.L., Jacobsen, S.B., 2001. Preservation of ancient and fertile lithospheric mantle beneath the southwestern United States. Nature 411, 69–72.

Liu, C.-Q., Masuda, A., Xie, G.-H., 1994. Major-and trace-element compositions of Cenozoic basalts in eastern China: petrogenesis and mantle source. Chem. Geol. 114, 19–42.

Liu, Y.-S., Gao, S., Jin, S.-Y., Hu, S.-H., Sun, M., Zhao, Z.B., Feng, J.L., 2001. Geochemistry of lower crustal xenoliths from Neogene Hannuoba basalt, North China Craton: implications for petrogenesis and lower crustal composition. Geochim. Cosmochim. Acta 65, 2589–2604.

Liu, Y., Gao, S., Yuan, H., Zhou, L., Liu, X., Wang, X., Hu, Z., Wang, L., 2004. U−Pb zircon ages and Nd, Sr, and Pb isotopes of lower crustal xenoliths from North China Craton: insights on evolution of lower continental crust. Chem. Geol. 211, 87–109.

Liu, Y., Gao, S., Lee, C.A., Hu, S., Liu, X., Yuan, H., 2005. Melt-peridotite interactions: links between garnet pyroxenite and high-Mg# signature of continental crust. Earth Planet. Sci. Lett. 234, 39–57.

Maalφe, A., Aoki, K., 1977. The major element composition of the upper mantle estimated from the composition of lherzolites. Contrib. Mineral. Petrol. 63, 161–173.

McCulloch, M.T., Gamble, J.A., 1991. Geochemical and geodynamical constraints on subduction zone magmatism. Earth Planet. Sci. Lett. 102, 358–374.

McDonough, W.F., 1990. Constraints on the composition of the continental lithospheric mantle. Earth Planet. Sci. Lett. 101, 1–18.

McDonough, W.F., Frey, F.A., 1989. Rare earth elements in upper mantle rocks. In: Lipin, B., McKay, G. (Eds.), Geochemistry and Mineralogy of Rare Earth Elements. Rev. Mineral., vol. 21, pp. 99–145.

Meisel, T., Walker, R.J., Irving, A.J., Lorand, J.-P., 2001. Osmium isotopic compositions of mantle xenoliths: a global perspective. Geochim. Cosmochim. Acta 65, 1311–1323.

Meng, Q.-R., 2003. What drove late Mesozoic extension of the northern China–Mongolia tract? Tectonophysics 369, 155–174.

Menzies, M.A., Zhang, M., Fan, W., 1993. Paleozoic and Cenozoic lithoprobes and the loss of >120 km of Archean lithosphere Sino-Korean Craton China. In: Prichard, H.M., Alabaster, T., Harris, N.B.W., Neary, C.R. (Eds.), Magmatic Processes and Plate Tectonics. Geol. Soc. Spec. Pub., vol. 76, pp. 71–78.

Mukasa, S.B., Shervais, J.W., 1999. Growth of subcontinental lithosphere: evidence from repeated dike injections in the Balmuccia lherzolite massif, Italian Alps. Lithos 48, 287–316.

Mukasa, S.B., Wilshire, H.G., 1997. Isotopic and trace element compositions of upper mantle and lower crustal xenoliths, Cima volcanic field, California: implications for evolution of the subcontinental lithospheric mantle. J. Geophys. Res. 102, 20133–20148.

Mukasa, S.B., McCabe, R., Gill, J.B., 1987. Pb-isotopic compositions of volcanic rocks in the west and east Philippine island arcs: presence of the Dupal isotopic anomaly. Earth Planet. Sci. Lett. 84, 153–164.

Mukasa, S.B., Shervais, J.W., Wilshire, H.G., Nielson, J.E., 1991. Intrinsic Nd, Pb, and Sr isotopic heterogeneities exhibited by the Lherz alpine peridotite massif, French Pyrenees. J. Petrol. Special Lherzolite, pp. 117–134. Volume.

Münker, C., Weyer, S., Scherer, E., Mezger, K., 2001. Separation of high field strength elements (Nb, Ta, Zr, Hf) and Lu from rock samples for MC-ICPMS measurements. Geochem. Geophys. Geosyst. 2. doi:10.1029/2001GC000183.

Navon, O., Stolper, E., 1987. Geochemical consequence of melt percolation: the upper mantle as a chromatographic column. J. Geol. 95, 285–307.

O'Reilly, S.Y., Griffin, W.L., Poudjom Djomani, Y.H., Morgan, P., 2001. Are lithospheres forever? Tracking changes in subcontinental lithospheric mantle through time. GSA Today 11, 4–10.

Palme, H., Nickel, K.G., 1985. Ca/Al ratio and compositions of the Earth's upper mantle. Geochim. Cosmochim. Acta 49, 2123−2132.

Patchett, P.J., Vervoort, J.D., Söderlund, U., Salters, V.J.M., 2004. Lu−Hf and Sm−Nd isotopic systematics in chondrites and their constraints on the Lu−Hf properties of the Earth. Earth Planet. Sci. Lett. 222, 29–41.

Pearson, D.G., Nowell, G.M., 2003. Dating mantle differentiation: a comparison of the Lu−Hf, Re−Os and Sm−Nd isotope systems in the Beni Bousera peridotite massif and constraints on the Nd−Hf composition of the lithospheric mantle. Geophys. Res. 05430 Abstracts 5.

Pearson, D.G., Nowell, G.M., 2004. Re−Os and Lu−Hf isotope constraints on the origin and age of pyroxenites from the Beni Bousera peridotite massif: implications for mixed peridotite–pyroxenite mantle sources. J. Petrol. 45, 439–455.

Pearson, D.G., Carlson, R.W., Shirey, S.B., Boyd, F.R., Nixon, P.H., 1995a. Stabilization of Archean lithospheric mantle: a Re−Os isotope study of peridotite xenoliths from the Kaapvaal craton. Earth Planet. Sci. Lett. 134, 341–357.

Pearson, D.G., Shirey, S.B., Carlson, R.W., Boyd, F.R., Pokhilenko, N.P., Shimizu, N., 1995b. Re−Os, Sm−Nd, and Rb−Sr isotope evidence for thick Archean lithospheric mantle beneath the Siberian craton modified by multistage metasomatism. Geochim. Cosmochim. Acta 59, 959–977.

Reisberg, L.C., Zindler, A., Jagoutz, E., 1989. Further Sr and Nd isotopic results from peridotites of the Ronda Ultramafic complex. Earth Planet. Sci. Lett. 96, 161–180.

Rudnick, R.L., Lee, C.-T., 2002. Osmium isotope constraints on tectonic evolution of the lithosphere in the southwestern United States. Int. Geol. Rev. 44, 501–511.

Rudnick, R.L., Gao, S., Ling, W., Liu, Y., McDonough, W.F., 2004. Petrology and geochemistry of spinel peridotite xenoliths from Hannuoba and Qixia, North China Craton. Lithos 77, 609–637.

Salters, V.J.M., 1996. The generation of mid-ocean ridge basalts from the Hf and Nd isotope perspective. Earth Planet. Sci. Lett. 141, 109−123.

Salters, V.J.M., White, W.M., 1998. Hf isotope constraint on mantle evolution. Chem. Geol. 145, 447−460.

Scherer, E.E., Cameron, K.L., Blichert-Toft, J., 2000. Lu−Hf garnet geochronology: closure temperature relative to the Sm−Nd system and the effects of trace mineral inclusions. Geochim. Cosmochim. Acta 64, 3413–3432.

Scherer, E.E., Münker, C., Mezger, K., 2001. Calibration of the lutetium–hafnium clock. Science 293, 683–687.

Shao, J., Liu, F., Chen, H., Han, Q., 2001. Relationship between Mesozoic magmatism and subduction in Dahingganling and Yanshan areas. Acta Geol. Sin. 75, 56–64.

Shearer, C.K., Papike, J.J., Simon, S.B., Shimizu, N., Yurimoto, H., Sueno, S., 1990. Ion microprobe studies of trace elements in Apollo 14 volcanic glass beads: comparison to Apollo 14 mare basalts and petrogenesis of picritic magma. Geochim. Cosmochim. Acta 54, 851–867.

Smith, A.D., 1998. The geodynamic significance of the DUPAL anomaly in Asia. In: Flower, M., Chung, S.-L., Lo, C.-H., Lee, T.Y. (Eds.), Mantle Dynamics and Plate Interactions in East Asia. Am. Geophys. Union, Geophys. Monogr., vol. 27, pp. 89–105.

Sneeringer, M., Hart, S.R., Shimizu, N., 1984. Strontium and samarium diffusion in diopside. Geochim. Cosmochim. Acta 48, 1589–1608.

Snow, J., Reisberg, L., 1995. Os isotope systematics of the MORB mantle: results from altered abyssal peridotites. Earth Planet. Sci. Lett. 133, 411–421.

Song, Y., Frey, F.A., 1989. Geochemistry of peridotite xenoliths in basalt from Hannuoba, Eastern China: implications for subcontinental mantle heterogeneity. Geochim. Cosmochim. Acta 53, 97–113.

Song, Y., Frey, F.A., Zhi, X., 1990. Isotopic characteristics of Hannuoba basalts, eastern China: implications for their petrogenesis and the composition of subcontinental mantle. Chem. Geol. 85, 35–62.

Sun, S.-S., McDonough, W.F., 1989. Chemical and isotopic systematics of oceanic basalts: implications for mantle composition and processes. Geol. Soc. London Spec. Publ., vol. 42 , pp. 313–345.

Takazawa, E., Frey, F.A., Shimizu, N., Obata, M., Bodinier, J.L., 1992. Geochemical evidence for melt migration and reaction in the upper mantle. Nature 359, 55–58.

Tatsumoto, M., Basu, A.R., Wankang, H., Junwen, W., Guanghong, X., 1992. Sr, Nd and Pb isotopes of ultramafic xenoliths in volcanic rocks and eastern China: enriched components EMI and EMII in subcontinental lithosphere. Earth Planet. Sci. Lett. 113, 107–128.

Toramaru, A., Fujii, N., 1986. Connectivity of melt phase in a partially molten peridotite. J. Geophys. Res. 91, 9239–9252.

Van Orman, J.A., Grove, T.L., Shimizu, N., 2001. Rare earth element diffusion in diopside: influence of temperature, pressure, and ionic radius, and an elastic model for diffusion in silicates. Contrib. Mineral. Petrol. 141, 687–703.

Vervoort, J.D., Blichert-Toft, J., 1999. Evolution of the depleted mantle: Hf isotope evidence from juvenile rocks through time. Geochim. Cosmochim. Acta 63, 533–556.

Walker, R.J., Prichard, H.M., Ishiwatari, A., Pimentel, M., 2002. The osmium isotopic composition of convecting upper mantle deduced from ophiolite chromites. Geochim. Cosmochim. Acta 66, 329–345.

Wells, P.R.A., 1977. Pyroxene thermometry in simple and complex systems. Contrib. Mineral. Petrol. 62, 129–139.

Wilshire, W.M., Shervais, J.W., 1975. Al-augite and Cr-diopside ultramafic xenoliths in basaltic rocks from the western United States. Phys. Chem. Earth 9, 257–272.

Wilde, S.A., Zhao, G.C., Sun, M., 2002. Development of the North China Craton during the late Archean and its final amalgamation at 1.8 Ga: some speculations on its position within a global Paleoproterozoic supercontinent. Gondwana Res. 5, 85–94.

Wilde, S.A., Zhou, X., Nemchin, A.A., Sun, M., 2003. Mesozoic crust–mantle interaction beneath the North China Craton: a consequence of the dispersal of Gondwanaland and accretion of Asia. Geology 31, 817–820.

Wilde, S.A., Zhou, X., Nemchin, A.A., Sun, M., 2006. SHRIMP U−Pb zircon ages from mafic-ultramafic xenoliths in the Cenozoic Hannuoba basalt, North China Craton: evidence for survival of Precambrian lithosphere. Western Pacific Geophysics Meeting, Beijing, 2006, p. 92. V35A-01.

Woodhead, J.D., Hergt, J.M., Davidson, J.P., Eggins, S.M., 2001. Hafnium isotope evidence for 'conservative' element mobility during subduction zone processes. Earth Planet. Sci. Lett. 192, 331–346.

Xu, Y., 2002. Evidence for crustal components in the mantle and constraints on crustal recycling mechanisms: pyroxenite xenoliths from Hannuoba, North China. Chem. Geol. 182, 301–322.

Yang, J.H., Wu, F.Y., Wilde, S.A., 2003. A review of the geodynamic setting of large-scale Late Mesozoic gold mineralization in the North China Craton: an association with lithospheric thinning. Ore Geol. Rev. 23, 125–152.

Zhai, M.G., 1996. Granulites and Lower Continental Crust in North China Archean Craton. Seismological Press, Beijing. 239 pp.

Zhang, H.-F., 2005. Transformation of lithospheric mantle through peridotite-melt reaction: a case of Sino-Korean craton. Earth Planet. Sci. Lett. 237, 768–780.

Zhang, M., Zhou, X.H., Zhang, J.B., 1998. Nature of the lithospheric mantle beneath NE China: evidence from potassic volcanic rocks and mantle xenoliths. In: Flower, M., Chung, S.-L., Lo, C.-H., Lee, T.Y. (Eds.), Mantle Dynamics and Plate Interactions in East Asia. Am. Geophys. Union, Geophys. Monogr., vol. 27, pp. 197–219.

Zhao, G., Cawood, P.A., Wilde, S.A., Sun, M., Lu, L., 2000. Metamorphism of basement rocks in the Central Zone of the North China Craton: implications for Paleoproterozoic tectonic evolution. Precambrian Res. 103, 55–88.

Zhao, G., Wilde, S., Cawood, P.A., Sun, M., 2001. Archean blocks and their boundaries in the North China Craton: lithological, geochemical, structural and $P-T$ path constraints and tectonic evolution. Precambrian Res. 107, 45–73.

Zheng, Z., O'Reilly, S.Y., Griffin, W.L., Lu, F., Zhang, M., 1998. Nature and evolution of Cenozoic lithospheric mantle beneath Shandong peninsula, Sino-Korean Craton, Eastern China. Int. Geol. Rev. 40, 471–499.

Zhi, X., Song, Y., Frey, F.A., Feng, J., Zhai, M., 1990. Geochemistry of Hannuoba basalts, eastern China: constraints on the origin of continental alkalic and tholeiitic basalt. Chem. Geol. 88, 1–33.

Zhou, X.H., Armstrong, R.L., 1982. Cenozoic volcanic rocks of Eastern China secular and geographic trends in chemistry and strontium isotopic composition. Earth Planet. Sci. Lett. 59, 301–329.

Zhou, X., Sun, M., Zhang, G., Chen, S., 2002. Continental crust and lithospheric mantle interaction beneath North China: isotopic evidence from granulite xenoliths in Hannuoba, Sino-Korean craton. Lithos 62, 111–124.

Zhu, B.Q., 1998. Theory and Applications of Isotope Systematics in Geosciences: Evolution of Continental Crust and Mantle in China. Science Press, Beijing. In Chinese.

Zindler, A., Hart, S., 1986. Chemical geodynamics. Annu. Rev. Earth Planet. Sci. 14, 493–571.

Zindler, A., Jagoutz, E., 1988. Mantle cryptology. Geochim. Cosmochim. Acta 52, 319–333.

Zou, H., Zindler, A., Xu, X., Qi, Q., 2000. Major, trace element, and Nd, Sr and Pb isotope studies of Cenozoic basalts in SE China: mantle sources, regional variations, and tectonic significance. Chem. Geol. 171, 33–47.